Rapid activation of tumor-associated macrophages boosts preexisting tumor immunity

Sabine Hoves,[1] Chia-Huey Ooi,[1,2] Carsten Wolter,[1] Hadassah Sade,[1] Stefan Bissinger,[1] Martina Schmittnaegel,[4] Oliver Ast,[3] Anna M. Giusti,[3] Katharina Wartha,[1] Valeria Runza,[1] Wei Xu,[3] Yvonne Kienast,[1] Michael A. Cannarile,[1] Hyam Levitsky,[3] Solange Romagnoli,[1] Michele De Palma,[4] Dominik Rüttinger,[1] and Carola H. Ries[1]

[1]Roche Pharmaceutical Research and Early Development, Roche Innovation Center Munich, Penzberg, Germany
[2]Roche Pharmaceutical Research and Early Development, Roche Innovation Center Basel, Basel, Switzerland
[3]Roche Pharmaceutical Research and Early Development, Roche Innovation Center Zurich, Schlieren, Switzerland
[4]Swiss Institute for Experimental Cancer Research, School of Life Sciences, École Polytechnique Fédérale de Lausanne, Lausanne, Switzerland

Depletion of immunosuppressive tumor-associated macrophages (TAMs) or reprogramming toward a proinflammatory activation state represent different strategies to therapeutically target this abundant myeloid population. In this study, we report that inhibition of colony-stimulating factor–1 receptor (CSF-1R) signaling sensitizes TAMs to profound and rapid reprogramming in the presence of a CD40 agonist before their depletion. Despite the short-lived nature of macrophage hyperactivation, combined CSF-1R+CD40 stimulation of macrophages is sufficient to create a proinflammatory tumor milieu that reinvigorates an effective T cell response in transplanted tumors that are either responsive or insensitive to immune checkpoint blockade. The central role of macrophages in regulating preexisting immunity is substantiated by depletion experiments, transcriptome analysis of ex vivo sorted TAMs, and gene expression profiling of whole tumor lysates at an early treatment time point. This approach enabled the identification of specific combination–induced changes among the pleiotropic activation spectrum of the CD40 agonist. In patients, CD40 expression on human TAMs was detected in mesothelioma and colorectal adenocarcinoma.

INTRODUCTION

Treatment of metastatic cancer patients with immunotherapies that unleash an ongoing T cell response against the tumor can be very effective and lead to long-lasting remissions (Hodi et al., 2010; Sharma and Allison, 2015; Topalian et al., 2015). However, only a subset of treated patients, particularly those with preexisting immunity, derive a substantial, durable clinical benefit from T cell checkpoint immunotherapy (Herbst et al., 2014; Tumeh et al., 2014; Rizvi et al., 2015). The abundant myeloid immune infiltrate that consists of tumor-associated macrophages (TAMs) and myeloid-derived suppressor cells (MDSCs) is thought to contribute to the escape from immune surveillance and checkpoint blockade therapy, as the tumor hijacks physiological mechanisms that normally restrain immune cell–mediated tissue damage (Coussens et al., 2013; Gajewski et al., 2013; Zhu et al., 2014; Holmgaard et al., 2016). The plastic nature of TAMs is based on their unique capability to activate a diverse functional repertoire in response to tissue-specific, local stimuli. Accordingly, TAMs have been described as either antitumorigenic (M1) or tumor promoting (M2) depending on the local milieu within different tumor types (Biswas and Mantovani, 2010; Gordon and Martinez, 2010; Ruffell and Coussens, 2015). TAMs represent

a frequent population that can suppress effector function of cytotoxic T cells and are therefore a highly attractive target for therapeutic intervention. Current approaches to block TAM activity in tumors focus on inhibiting CSF-1–regulated activation of its cognate receptor, CSF-1R, thereby affecting recruitment, differentiation, and survival of TAMs (Lin et al., 2001; MacDonald et al., 2010). In mouse models of cancer, CSF-1R blockade reduced TAM-mediated T cell and dendritic cell (DC) suppression and synergized with T cell–activating therapies such as adoptively transferred T cells and checkpoint inhibitors (Mok et al., 2014; Ruffell et al., 2014; Zhu et al., 2014; Eissler et al., 2016; Holmgaard et al., 2016; Marigo et al., 2016). In addition, we previously described an anti–human CSF-1R therapeutic antibody (RG7155, emactuzumab) that reduced the TAM infiltrate in cancer patients and shifted the CD8/CD4 T cell ratio in favor of CD8^{+} effector T cells (Ries et al., 2014).

An alternative therapeutic approach to target TAMs involves the reprogramming of TAMs toward an antitumoral, classically activated M1 phenotype. Accordingly, blockade of PI3K-γ was described to result in TAM reprogramming by reducing the M2-associated characteristics of TAMs (De Henau

et al., 2016; Kaneda et al., 2016). Mechanistically, this concept was further supported by genetic loss of endoribonuclease Dicer expression in TAMs that resulted in an M1-skewed TAM infiltrate and an increased antitumoral cytotoxic T cell response (Baer et al., 2016). Interestingly, CSF-1R blockade has been accounted for reprogramming those remaining TAMs that were not depleted by the CSF-1R small molecule inhibitor PLX3397 (Zhu et al., 2014). Notably, this CSF-1R inhibitor not only has an impact on TAMs but also on MDSCs, which are also known to inhibit T cell effector functions. Treatment of tumors in mice with PLX3397 resulted in reduced MDSC recruitment and reprogramming toward an antigen-presenting, immunostimulatory phenotype with enhanced antitumoral T cell responses in combination with an antibody targeting CTLA-4 (Holmgaard et al., 2016). Similar observations of enhanced MHC II^hi proinflammatory TAM differentiation have been reported recently for combining a CSF-1R–blocking antibody with a CD40 agonist (Wiehagen et al., 2017).

Strong activation of the M1 phenotype in macrophages requires two signals. After priming by, e.g., IFN-γ, which leads to TLR up-regulation, an additional triggering signal initiates a maximal cytotoxic macrophage response. Triggering signals can consist of LPS or other pathogen-associated molecular patterns (Schroder et al., 2004; Rakhmilevich et al., 2012). In addition, CD40 agonists can also serve as a priming signal leading to up-regulation of TLR. Accordingly, a combination therapy using CD40 ligation together with the TLR9 agonist CpG resulted in synergistic antitumoral activity (Guiducci et al., 2005; Buhtoiarov et al., 2006).

CD40, a member of the TNF receptor family, is broadly expressed on many cell types including all APCs, B cells, DCs, and macrophages, as well as endothelial cells and tumor cells (Grewal and Flavell, 1998; Eliopoulos and Young, 2004; Fonsatti et al., 2010). CD40 signaling is initiated by the engagement of CD40L expressed mainly on activated T helper cells (Th cells), which induces receptor trimerization. Upon CD40 ligation, APCs secrete proinflammatory cytokines and up-regulate costimulatory molecules such as CD80 and CD86 that are required for costimulation via CD28 on CD8 effector T cells (Elgueta et al., 2009). However, T cell–independent antitumoral effects that involve tumoricidal macrophages have also been described (Suttles and Stout, 2009; Beatty et al., 2011). The need for CD40 ligation can be bypassed by using agonistic anti-CD40 antibodies that mediate CD40 trimerization via FcγR engagement. In mouse models, the FGK.45 antibody is used to activate CD40 via cross-linking by FcγRIIB (Li and Ravetch, 2011; Vonderheide and Glennie, 2013). However, contradictory findings were also reported on the FcγR-dependent agonistic activity of anti–human CD40 antibodies of the human IgG2 isotype that poorly binds to FcγR (Richman and Vonderheide, 2014; Dahan et al., 2016).

Preclinical evaluation of CSF-1R inhibitors not only demonstrated reprogramming of the remaining TAMs and MDSCs, but also revealed that the process of TAM depletion is not immediate and instead requires up to 8 d (Zhu et al., 2014). Therefore, we asked whether combination with a CD40 agonist represents a viable strategy to maximize the CSF-1R blockade–induced reprogramming effects on myeloid cells. To this end, we used transplanted, immunogenic tumor models with a rich infiltrate of TAMs and T cells and initiated treatment at a large tumor size to allow sufficient time for complete TAM differentiation. This dual TAM-targeting combination is also currently being assessed in an early clinical trial (ClinicalTrials.gov identifier NCT02760797).

RESULTS

Combination of a CSF-1R inhibitor with a CD40 agonist leads to tumor rejection

TAM reprogramming has been documented previously in prolonged treatment with CSF-1R small molecule inhibitors (Pyonteck et al., 2013; Zhu et al., 2014). However, at the time points evaluated in these studies, TAMs were either already depleted or still present on account of the glioma-specific environment. Here, we performed transcriptome analysis of tumors that had been treated for only 16 h to gain deeper insight into TAM reprogramming by CSF-1R blockade at a very early phase. We chose the MC38 adenocarcinoma model and treated with an anti–mouse CSF-1R antibody (αCSF-1R) in the short term, which shows comparable affinity to the clinically tested human CSF-1R–blocking antibody emactuzumab (RG7155; Ries et al., 2014). When we compared the statistically significant changes in gene expression induced by αCSF-1R with signatures of all types of cells (Table S1), we found that genes associated with general activation were up-regulated and genes associated with general suppression were down-regulated in these tumors by αCSF-1R treatment (Fig. 1 A and Table S1). Reduced expression of *GrzD*, *GrzF*, and *GrzK* may reflect the decrease of TAM frequency in whole tumor lysates, as orphan granzymes were reported to be expressed not only by T or natural killer (NK) cells but also by myeloid cells such as plasmacytoid DCs (Bovenschen and Kummer, 2010). To further enhance the observed activation phenotype by αCSF-1R monotherapy, we combined the CSF-1R inhibitor with an anti-CD40 antibody (αCD40) that is also known to activate TAMs (Beatty et al., 2011). MC38 tumors were treated at various tumor volumes (small, day 7, ∼80 mm³; large, day 11, ∼200 mm³), based on previous studies demonstrating improved antitumoral efficacy of αCD40 monotherapy at bigger tumor volumes (Tutt et al., 2002). In both settings, the combination therapy showed significantly improved antitumor responses and even tumor regression when compared to either of the monotherapies (Fig. 1 B and Table S2; asterisks in Table S2 indicate significance independent of the actual p-value). Whereas in the small tumor setting, only 2/10 mice showed complete tumor regression, 6/10 of mice were tumor free after αCSF-1R+αCD40 combined treatment when starting with larger tumors. However, this increase in response rate was mainly driven by enhanced activity of the CD40 agonist that regressed the larger tumors

in monotherapy in 2/10 mice (Fig. 1 B and Fig. S1 C). Summarizing all studies that have been performed under similar conditions (tumor volume at start >100 mm^3), 68% of animals (47/70) that had received combined αCSF-1R+αCD40 treatment were tumor free (Fig. S1 A). In addition, we found that both combination partners in the small tumor setting had to be administered simultaneously, whereas sequencing of αCSF-1R and αCD40 did not show any impact on the number of tumor-free mice in the large tumor setting (Fig. S1 B). Notably, sole depletion of CD8$^+$ T cells in MC38 tumors resulted in enhanced tumor growth, indicating an ongoing T cell response against the MC38 tumor cell line (Fig. 1 C). However, a monotherapy using αPD-1 antibody or a combination together with anti–CTLA-4 antibody did not improve survival of mice when large tumors were treated (Fig. 1, D and E; and Fig. S1 D). A previous study further suggested that the administration route of the CD40 agonist could also influence its efficacy (Sandin et al., 2014). Analysis of the pharmacokinetic (PK) profile of αCD40 revealed that differences in the application are visible only at early time points in the periphery (0–10 h after administration and evaluated by eye imaging) and in the tumor itself (Fig. S2, A, C, and D). This was most prominent when αCD40 was given i.v., compared with s.c. and i.p. application, as expected. The distribution of αCD40 also matched the number of activated CD69$^+$ B cells in peripheral blood and B cell redistribution into the tissue 1 h after antibody administration (Fig. S2 B). No differences were seen in the frequency of tumor-free mice by αCSF-1R+αCD40 combination treatments using different application routes for the αCD40 antibody (Fig. S2 E). To investigate whether the synergistic activity of the combination was restricted to tumor models with a high TAM infiltrate, we additionally evaluated E0771 and T241 murine tumor cell lines. The E0771 and T241 model showed enhanced antitumoral activity by combination compared to monotherapies, resulting in a smaller fraction of tumor-free mice and delayed tumor growth, albeit with lower response rates compared to the MC38 model (Fig. 1 F and Fig. S1 C). Collectively, these results indicate that the αCSF-1R+αCD40 dual therapy elicits an antitumoral benefit in different transplanted tumor models and even in large-sized MC38 tumors demonstrated to be resistant to immune checkpoint blockade.

TAMs are required for the synergistic αCSF–1R+αCD40 combination effect

The differences in antitumoral efficacy of the combination in the small versus large MC38 tumors prompted us to characterize the myeloid tumor infiltrate in more detail (Fig. S3 A). Flow cytometry revealed that the infiltrate of larger tumors (day 11) was dominated by a monocytic/TAM infiltrate, which we classified into three major subpopulations: TAM (CD11b$^+$F4/80^{hi}Ly6C^{low}Ly6G^{neg}), monocytic MDSC (CD11b$^+$F4/80$^{-/low}$Ly6C^{hi}Ly6G^{neg}), and an MDSC–TAM intermediate population referred to as Ly6C^{low} MDSC (CD11b$^+$F4/80$^{-/low}$Ly6C^{low}Ly6G^{neg}), which might represent

a TAM precursor population (Ries et al., 2015; Baer et al., 2016). Granulocytic MDSCs (CD11b$^+$F4/80$^{-/low}$Ly6C^{inter}Ly6G^{high}) contributed little to the myeloid infiltrate at day 11 (Fig. S3 A). The most striking difference between the two tumor sizes was that at day 7, the myeloid infiltrate was dominated by MDSCs, which might be indicative of increased TAM maturation during tumor growth. Notably, the total lymphoid infiltrate remained unchanged (Fig. S3 A). Despite the observed differences in myeloid cell maturation, CD40 expression on TAM did not change, whereas PD-L1 expression increased along with the tumor growth (Fig. S3 B).

Next, we analyzed the tumor immune infiltrate upon treatment with the αCSF-1R+αCD40 combination on day 10 after treatment (Fig. 2, A and B; and Fig. S3 C). As previously reported (Ries et al., 2014), αCSF-1R led to a dramatic decrease of TAMs and TAM precursors, in contrast to monocytic MDSCs, which were only partially reduced after CSF-1R inhibition. This finding underscores the relevance of CSF-1R signaling at a rather late stage of differentiation in the monocytic lineage. Both populations, TAMs and TAM precursors, were also equally reduced in αCSF-1R+αCD40 combined treatment. However, αCD40 was able to abolish the αCSF-1R–mediated mild reduction of the monocytic MDSCs. Both monotherapy groups with αCSF-1R and αCD40 increased granulocytic MDSCs and resulted in an additive increase upon combination treatment (Fig. 2 A). The αCD40 agonist alone showed its most pronounced effect by elevating intratumoral CD8$^+$ T cell frequency. Moreover, combination treatment showed a slight increase in CD8$^+$ T cells and NK cells, but also in FoxP3$^+$ regulatory T cells (T reg cells; Fig. 2 B).

Based on the flow cytometry data showing nearly complete TAM eradication in these tumors, we wanted to test how long the depletion of TAM needed to persist for tumor regression. Therefore, we compared continuous, weekly TAM depletion to a single dose or two doses of αCSF-1R together with αCD40. Surprisingly, we detected comparable antitumoral responses in all combinatorial treatment groups (Fig. 2 C). This indicates that the benefit of the combination effect might not lie in the continuous removal of TAMs from the tumor microenvironment. Moreover, the trigger for tumor regression seems to be initiated with the first dose of both αCSF-1R and αCD40 antibodies. PK analysis of αCSF-1R antibody exposure in peripheral blood showed a pronounced decline 9 d after initial antibody application (Fig. S3 D).

To dissect the effect of TAMs in the combined setting, we depleted TAMs from MC38 tumor–bearing mice before αCSF-1R+αCD40 combination treatment. Of note, the αCD40 clone FGK.45 used in this study is known to require FcγRIIb for cross-linking to mediate CD40 activation (Li and Ravetch, 2011; Richman and Vonderheide, 2014). Our initial experiments showed that the αCD40 monotherapy effect was reduced in animals that were pretreated with mIgG1 (Fig. 2 D and Fig. S3 E), indicating that high and stable IgG levels might hinder FcγR-dependent cross-linking. There-
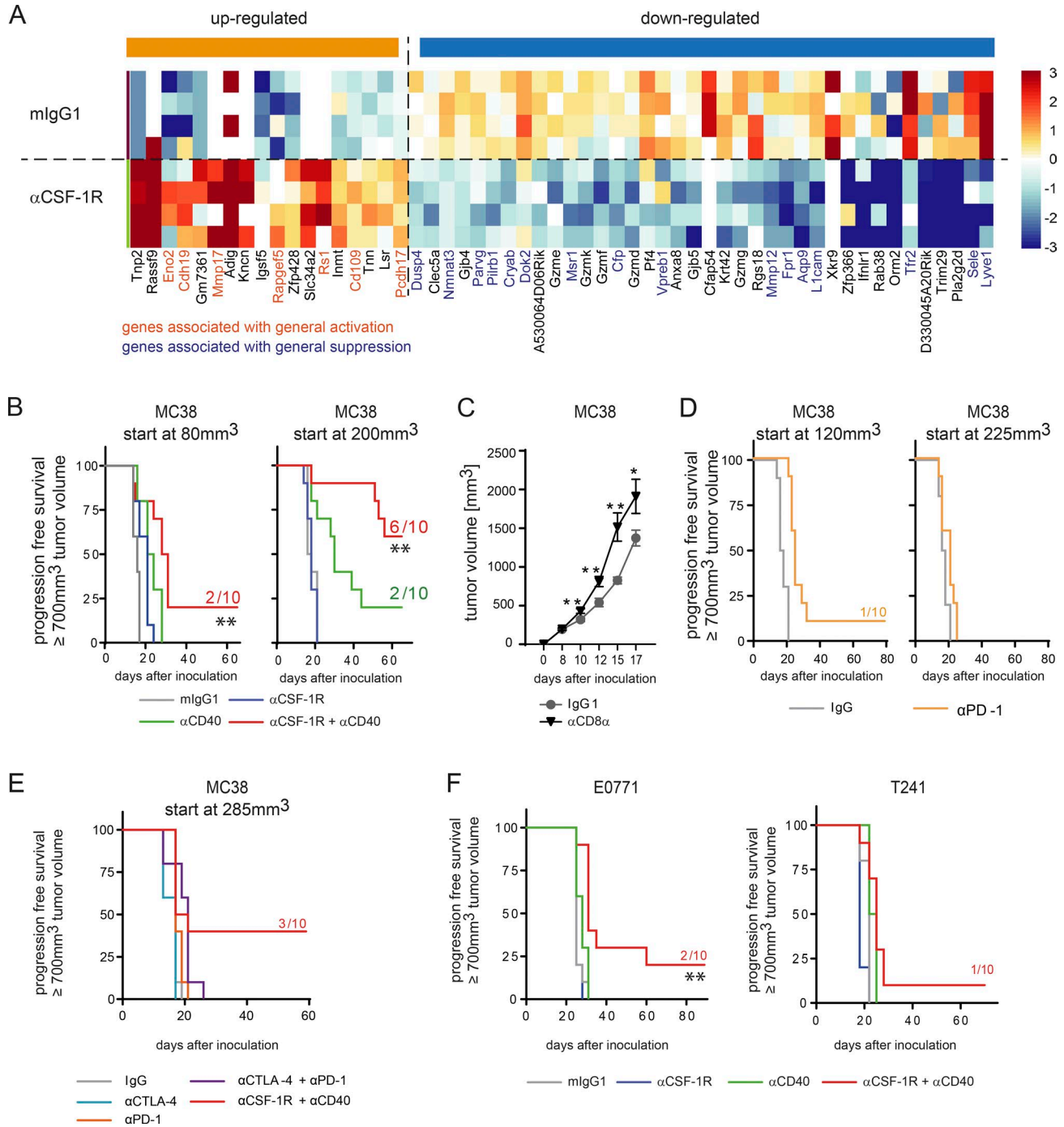
Figure 1. **Combination of CSF–1R inhibition and αCD40 treatment leads to rejection of MC38 tumors. (A)** αCSF-1R treatment indicates up-regulation of genes belonging to activation signatures. Single-cell suspension of whole tumors was obtained 16 h after in vivo treatment with either mIgG1 or αCSF-1R (30 mg/kg; $n = 4$ each; tumors were treated on day 10 and 11, respectively, after inoculation at a mean tumor volume of ~200 mm^3), and RNA sequencing was performed. Data were compared with activation signatures (Table S1), and genes regulated by αCSF-1R compared with control belong to at least one of the general activation signatures (genes marked in orange are associated with general activation, and genes marked in blue are associated with suppression). **(B)** MC38 tumor–bearing mice were treated using 30 mg/kg mIgG1, 30 mg/kg αCSF-1R weekly, 4 mg/kg αCD40 once, or a combination of both targeting antibodies, starting treatment at either 80 mm^3 or 200 mm^3 tumor volume. **(C)** MC38 tumor–bearing mice were either treated with 30 mg/kg mIgG1 ($n = 10$) or four times with 4 mg/kg of an anti-CD8α antibody ($n = 9$) to deplete CD8$^+$ T cells. Isotype control treatment started on day 10, and the anti-CD8α treatment was given on days 7, 9, and 11. Graphs show mean ± SEM of tumor volumes and statistical analyses by two-tailed Student's t test for each time point depicted. **(D)** MC38 tumor–bearing mice were treated using 30 mg/kg mIgG1 or 10 mg/kg αPD-1 (three times a week for 2 wk), starting treatment at either 120 mm^3 or 225 mm^3 tumor volume. **(E)** MC38 tumor–bearing mice were treated using 30 mg/kg mIgG1, 4 mg/kg αCTLA-4 weekly, 10

fore, we generated an FcγR–nonbinding (FcØ) version for both antibody clones of IgG1 and αCSF-1R (Schlothauer et al., 2016). Pretreatment with either fully FcγR–competent mIgG1, IgG1-FcØ, or αCSF-1R–FcØ of mice bearing MC38 tumors was conducted on days 3 and 9 after tumor cell inoculation, and TAM depletion was confirmed by flow cytometry (Fig. S3 F). Indeed, the absence of TAM completely abrogated the antitumoral effects of the combination therapy, whereas pretreatment of tumor-bearing mice with isotype controls resulted in tumor rejection in 7/10 mice when treated with the αCSF-1R+αCD40 combination (Fig. 2 D). Importantly, αCSF-1R–FcØ achieved comparable numbers of tumor-free mice as the parental, FcγR–competent antibody αCSF-1R when combined with αCD40 (Fig. 2 D). These data underline that macrophages are key for mediating the beneficial effect of the αCSF-1R+αCD40 combination.

CSF-1R inhibition amplifies αCD40–mediated TAM reprogramming toward a strong proinflammatory phenotype

To gain further insight into the TAM-regulated processes that enable MC38 tumor rejection after combination therapy, we sorted TAMs and monocytic MDSCs for transcriptome analysis from tumors treated for 16 h with the combination or matching monotherapies (Fig. 3, A and B). In both myeloid populations, we found genes that were strongly up-regulated only in the αCSF-1R+αCD40 cohort resembling an M1-like macrophage phenotype when compared with general activation signatures from different cell types stimulated with LPS, TNF-α, or IFNs (Table S1). As expected, αCD40 treatment alone was confirmed to be a strong regulator of proinflammatory gene expression in both myeloid populations analyzed.

To confirm the results obtained by RNA sequencing, we repeated the experiment and detected mRNA transcripts by a quantitative and multiplexed method referred to as NanoString nCounter Gene Expression Assay from whole tumors (Kulkarni, 2011). Using both methods, RNA sequencing analyses of flow cytometry–sorted TAMs and NanoString of whole tumor lysates, we detected a substantial overlap in terms of increased proinflammatory signatures in the combination group (Table S3). In-depth analyses of NanoString data were performed based on genes typically considered important and involved in general immune and cell type–specific regulation that were selected for significant regulation in the combination cohort compared with either monotherapy (Fig. 3 C and Fig. S4 A). We uncovered enhanced activation of αCD40-induced alternatively activated NF-κB signaling and down-regulation of inhibitory receptors

expressed on peripheral mononuclear cells such as *Lair1* and *Trem2*. Consistently, we observed increased M1 marker expression (*Nos2*, *Il1b*, and *IL-12*) and IFN signaling–regulated genes *Irf1* and *Irf8*, which are critical for myeloid differentiation and amplification of IFN signals (Hu and Ivashkiv, 2009; Langlais et al., 2016). Moreover, we found reduced expression of the M2 macrophage–associated genes *Msr1* and *Itgax* (Fig. S4 A), which was previously described to be down-regulated upon TLR activation (Singh-Jasuja et al., 2013). With regard to APCs, an increased mRNA signal was detected for *Cd83*, *Cd80*, *Cd86*, and *β2m*, whereas the transcription factor of cross-presenting DC *Batf3* remained unchanged (Fig. S4 A; Murphy et al., 2013). Together with an enhanced M1 phenotype of TAM, genes were up-regulated that were associated with a Th1 cell response, including T cell activation and enhanced recruitment such as GrzA, GrzB, Prf1, Cxcl10, Ccl5, and Vcam1. Notably, we did not detect alterations in *Cd8a/b* and *Ifng* mRNA levels by NanoString at this early time point, which was optimized to characterize the immediate effects of the combination therapy on the myeloid cells. As a possible physiological compensatory mechanism in response to the strong inflammatory signature, an increase in the checkpoint inhibitor *Pdl1* but not *Pdcd1* expression was detected, along with increased levels of genes associated with T reg cells such as *Ccl22* and *Foxp3* (Fig. 3 C and Fig. S4 A; Guiducci et al., 2005; Jenabian et al., 2014). Importantly, these combination-induced gene transcriptional changes were validated by augmented protein expression of the proinflammatory cytokines IL-1β, IL-12p40, and IL-27 as well as the chemokines CCL2, CCL5, and CCL22 in whole tumor lysates compared with either monotherapy (Fig. 3 D). When we assessed the transcriptional changes in isolated TAMs in comparison to the protein expression alterations in whole tumor lysates, we noticed that both the proinflammatory cytokine IL-27 and the T cell–recruiting chemokine CCL5 shared an identical up-regulation in the combination group. Hence, we concluded that TAMs are likely a source for these factors (Table S1). However, we were not able to detect increased *IL1b* mRNA expression, either in sorted TAM or in MDSC populations, whereas IL-1β mRNA and protein levels were strongly increased in whole tumor lysates, suggesting other cellular sources than TAMs and a general immune activation. The observed NF-κB pathway activation is consistent with increased IL-1β levels. Finally, these gene transcriptional changes were validated by an increase in the MHC II protein level on TAMs after 3 d of combination therapy by flow cytometry. Although αCD40 induced an MHC II increase

---

mg/kg αPD-1 once, or a combination of both targeting antibodies as well as 4 mg/kg αCD40 once plus 30 mg/kg αCSF-1R weekly, starting treatment at 285 mm³ tumor volume. **(F)** C57BL/6 mice were inoculated with the indicated syngeneic tumors E0771 and T241 (*n* = 10 per group and model) and were treated using mIgG1, αCSF-1R, αCD40, or a combination of both targeting antibodies. (B and D–F) Animals were graphically censored in Kaplan-Meier curves once the tumor volume reached ≥700 mm³, and the numbers in graphs indicate the amount of tumor-free mice within the specific group (*n* = 10 for all groups depicted). Asterisks indicate log-rank tests between αCD40- and αCSF-1R+αCD40–treated animals, and detailed log-rank test results for the other groups are available in Table S2; all animal survival experiments (B–F) were performed at least twice. *, P < 0.05; **, P < 0.01.
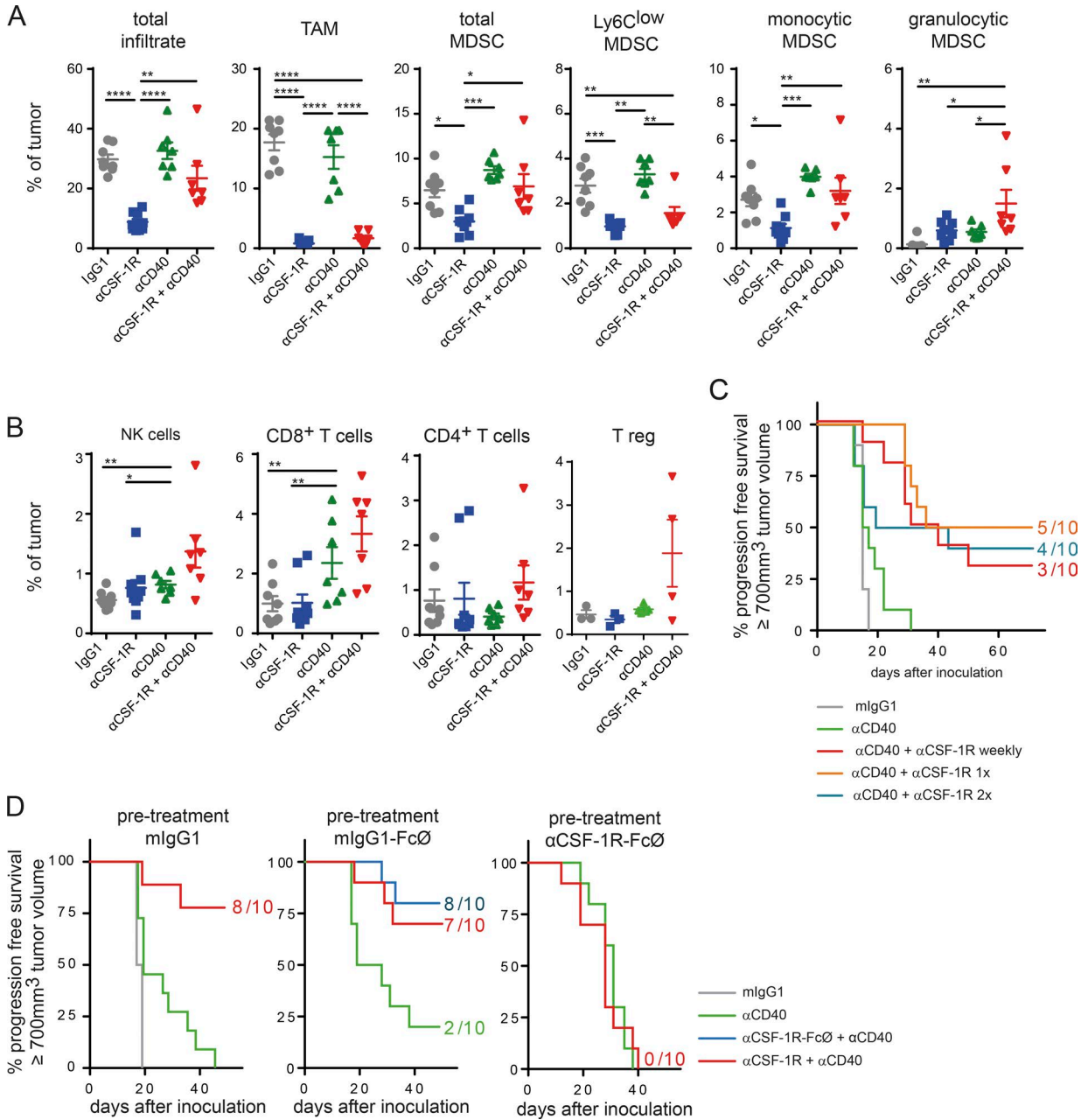
Figure 2. **TAMs are required for αCSF–1R+αCD40–mediated tumor rejection. (A and B)** Immune infiltrate of MC38 tumors on day 10 upon start of treatment. MC38 tumor–bearing mice were treated with either 30 mg/kg mIgG1, 30 mg/kg αCSF-1R weekly, 4 mg/kg αCD40 once, or a combination of both targeting antibodies. Data shown in A and B are pooled from two independent experiments, and T reg cells were assessed in the third experiment. Graphs show means ± SEM; statistical analysis by one-way ANOVA and Tukey correction (*, P < 0.05; **, P < 0.01; ***, P < 0.001; ****, P < 0.0001). **(C)** A single combined dose of αCSF-1R and αCD40 antibodies is sufficient for tumor rejection. MC38 tumor–bearing mice were treated using 30 mg/kg mIgG1, 4 mg/kg αCD40 once, or in combination with 30 mg/kg αCSF-1R given weekly (four times total), once (first treatment day), or twice on first and second treatment day. This experiment is exemplary out of two independent experiments. **(D)** Predepletion of macrophages completely abolishes tumor rejection in MC38 tumor–bearing mice. Mice were inoculated with MC38 tumors and received on days 3 and 9 upon inoculation of either 30 mg/kg mIgG1, mIgG1 incompetent in binding to FcγR (mIgG1-FcØ), or αCSF-1R clone 2G2 incompetent in binding to FcγR (αCSF-1R–FcØ). On day 11, at a mean tumor volume of 120 mm³, mice were treated with a single dose of either 130 mg/kg mIgG, 4 mg/kg αCD40, or a combination of 30 mg/kg αCSF-1R+αCD40 (FcγR competent or incompetent versions). Depletion of TAMs was confirmed by flow cytometry on day 11 from scout animals (Fig. S3 D). (C and D) Mice were graphically censored once the tumor size reached ≥700 mm³, and numbers in graphs indicate the amount of tumor-free mice within the specific group from n = 10 for all groups depicted.

864

Short-term TAM hyperactivation by anti–CSF-1R+CD40 | Hoves et al.
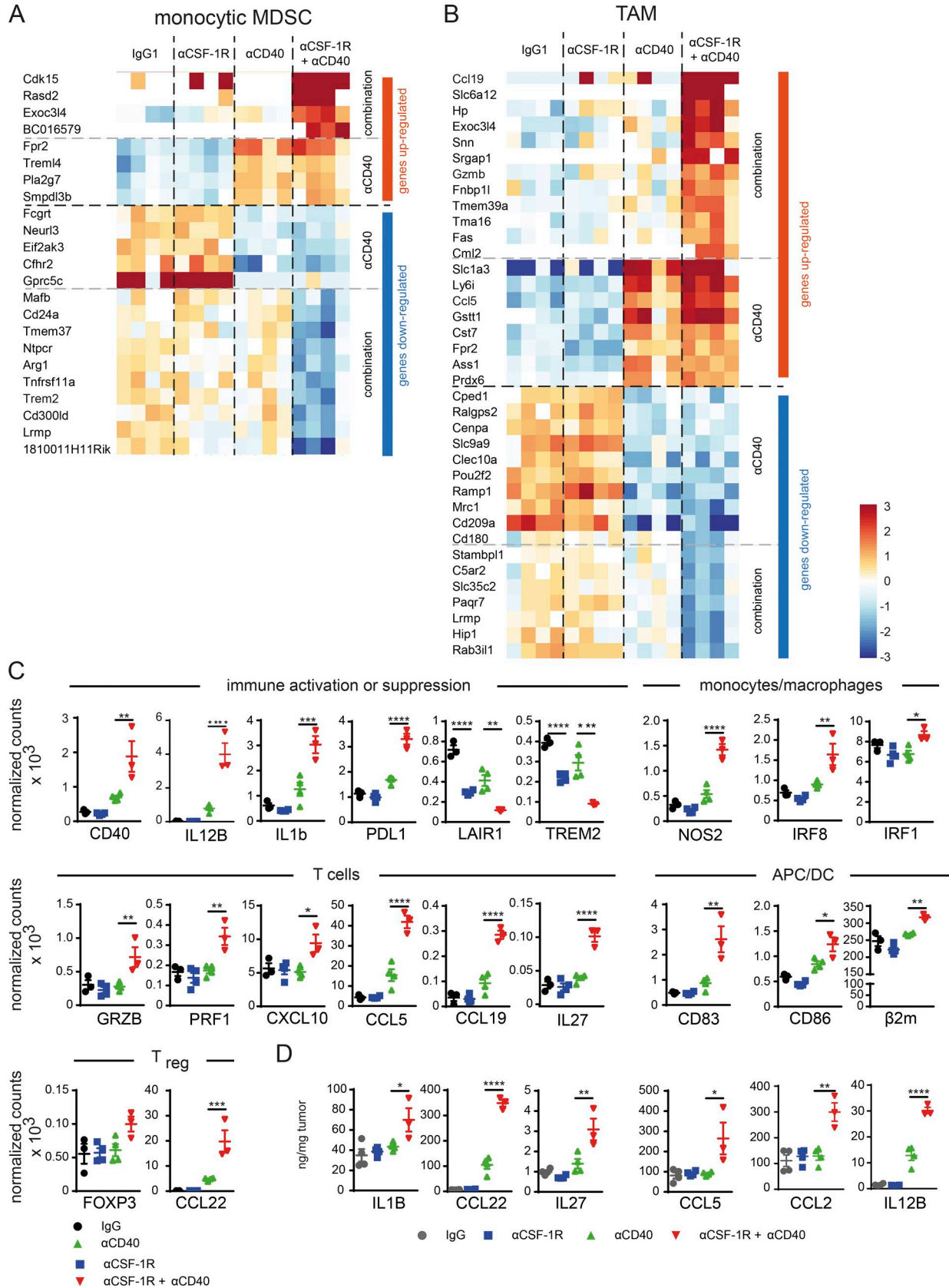
similar to αCSF-1R+αCD40 combination in the spleen, significantly higher MHC II expression was only sustained in tumors from the αCSF-1R+αCD40 group (Fig. S4 B). Together, these data provide further evidence that activation via αCD40 in concert with CSF-1R blockade promote a strong proinflammatory phenotype of TAMs associated with general immune and T cell activation and recruitment. Of note, most of these combination therapy–mediated changes indicate that CSF-1R inhibition enhanced the CD40 agonist–induced alterations in RNA and protein expression.

## Tumor rejection via αCSF-1R+αCD40 combination depends on effector T cells

The gene expression profiling of whole tumors by Nano-String analysis indicated a clear involvement of T cells and their activation upon αCSF-1R+αCD40 therapy. We next analyzed in more detail the role of effector T cells in promoting this strong antitumoral effect. To address whether tumor rejection resulted in the formation of immunological memory, we rechallenged tumor-free mice by inoculating MC38 cells into the contralateral flank of the initial tumor. After a short initial period of tumor growth, all mice also rejected the second tumor, suggesting formation of a memory T cell response during the first tumor rejection (Fig. 4 A).

Next, we evaluated de novo priming by αCSF-1R+αCD40 treatment of cytotoxic T cells by using an adoptive transfer of naive OT-I cells in mice bearing tumors of an OVA-expressing MC38 line variant (MC38-OVA). OT-I cells were analyzed by flow cytometry on day 3 after αCSF-1R+αCD40 treatment for proliferation and changes in the activation status by CD44/CD62L expression. This combination significantly increased proliferation of OVA-specific CD8$^+$ T cells and frequency of effector memory OT-I in the spleen, but not with the αCD40 treatment alone (Fig. S4 C). The observation of enhanced, tumor-specific T cell responses along with augmented RNA levels of (a) *Cd83*, a DC maturation marker, (b) *β2m*, a component of the MHC class II complex, and (c) *CCR7*, as

well as its ligand *CCL19*, which is involved in lymph node homing of DCs (Fig. 3 C), motivated a comprehensive analysis of the DC population. Although no differences in the frequencies of total CD24$^+$ DCs were detected in the combination-treated tumors, a relative increase in the migratory CD103$^+$ DC population became evident (Fig. S4 D). The increased migratory DC/all DC ratio is consistent with an increase of *Irf8* and *Ccr7* expression (Fig. 3 C and Fig. S4 C; Tamura and Ozato, 2002). Analysis of spleens treated with the CSF-1R inhibitor for 10 d indicated no decrease of DCs, whereas F4/80$^+$ macrophages were reduced, albeit to a lesser extent than in tumors (Fig. S4 E). Further analysis of the responsive tumor models MC38, E0771, and T241 on day 10 after αCSF-1R+αCD40 treatment showed similar effects on endogenous CTLs in the spleen (Fig. 4 B). In the strongly responsive MC38 model, the combination treatment in particular resulted in significantly increased numbers of activated central memory CTLs (activated CTL/CTL$_{CM}$) and effector memory CTLs, whereas no increase in T reg cells was detected (Fig. 4 B). Notably, analysis of effector T cells in the spleen of the models E0771 and T241 that were responsive to αCSF-1R+αCD40 treatment (Fig. 1 F) demonstrated a similar increase as seen in the MC38 model, albeit with no effects on the CTL$_{CM}$ population (Fig. 4 B).

To finally link tumor rejection and the changes in the CTL activation phenotype (Fig. 4 B), we depleted CD4$^+$ and CD8$^+$ T cells before starting the αCSF-1R+αCD40 treatment in MC38 tumors. We also included NK cell depletion, as previous studies described a role for NK cells in αCD40-mediated antitumoral activity and an increased NK cell infiltrate detected after αCSF-1R treatment (Nakajima et al., 1998; Ries et al., 2014). Depletion of CD8$^+$ T cells completely abrogated the beneficial survival effect in αCSF-1R+αCD40-treated mice. Neither CD4$^+$ T nor NK cell depletion had an impact on the survival of these mice (Fig. 4 C). Collectively, these findings demonstrate that, in addition to the key contribution of repolarized TAMs (Fig. 2 D), a cytotoxic T cell response is additionally needed

Figure 3. **CSF-1R inhibition accelerates αCD40–mediated TAM reprogramming toward a strong proinflammatory phenotype. (A and B)** Monocytic MDSCs and TAMs were sorted from tumors 16 h after treatment using 30 mg/kg mouse IgG1 + 4 mg/kg rat IgG2a, 30 mg/kg αCSF-1R rat + 4 mg/kg IgG2a, 4 mg/kg αCD40 + 30 mg/kg IgG1, or a combination of both targeting antibodies, and RNA sequencing was performed (*n* = 4 each). Heat maps show genes up- or down-regulated, driven by either αCD40 alone (compared to IgG and αCSF-1R) or only occurring in the combination of αCSF-1R+αCD40 (compared with IgG, αCD40, and αCSF-1R). Genes depicted were also found by either being a member of M1- and/or M2-related signatures described in Table S1, or by being differentially regulated in M1 versus M2 based on a gene expression dataset comprising activated M1 and M2a macrophages GSE5099 (Martinez et al., 2006) and GSE58318 (Kaneda et al., 2016). Criteria for differential regulation: absolute log2 ratio >1 and an adjusted p-value <0.05. P-values were derived using R function aov() (Gentleman and Ihaka, 2017). Genes with contradicting information on direction of regulation (e.g., up-regulated in M2 according to one source but down-regulated in M2 in another source) were eliminated from the visualization. To determine genes regulated by combination (vs. IgG, αCSF-1R, and αCD40), p-values were computed using R function aov() with Tukey correction for multiple comparison of treatment groups. Genes were deemed as specifically regulated by combination if there was differential expression between combination and all monotherapies (P < 0.05 and absolute log2 ratio >1). **(C)** Selected genes from NanoString analysis of whole tumor tissue from treatment groups at the same time point as A and B, expressed as counts normalized to housekeeping genes *Ppia*, *Polr2a*, *Eef1g*, *Sdha*, and *Rpl19*. **(D)** Protein data of selected cytokines and chemokines from treatment groups at the same time point as A–C by ELISA or by multiplex bead assay from whole tumor tissue. (C and D) Data are depicted as means ± SEM and analyzed using one-way ANOVA and Tukey correction. P-values are shown only for the comparison of αCD40 with αCSF-1R+αCD40, unless αCSF-1R treatment alone had significant impact on mRNA levels (*, P < 0.05; **, P < 0.01; ***, P < 0.001; ****, P < 0.0001).
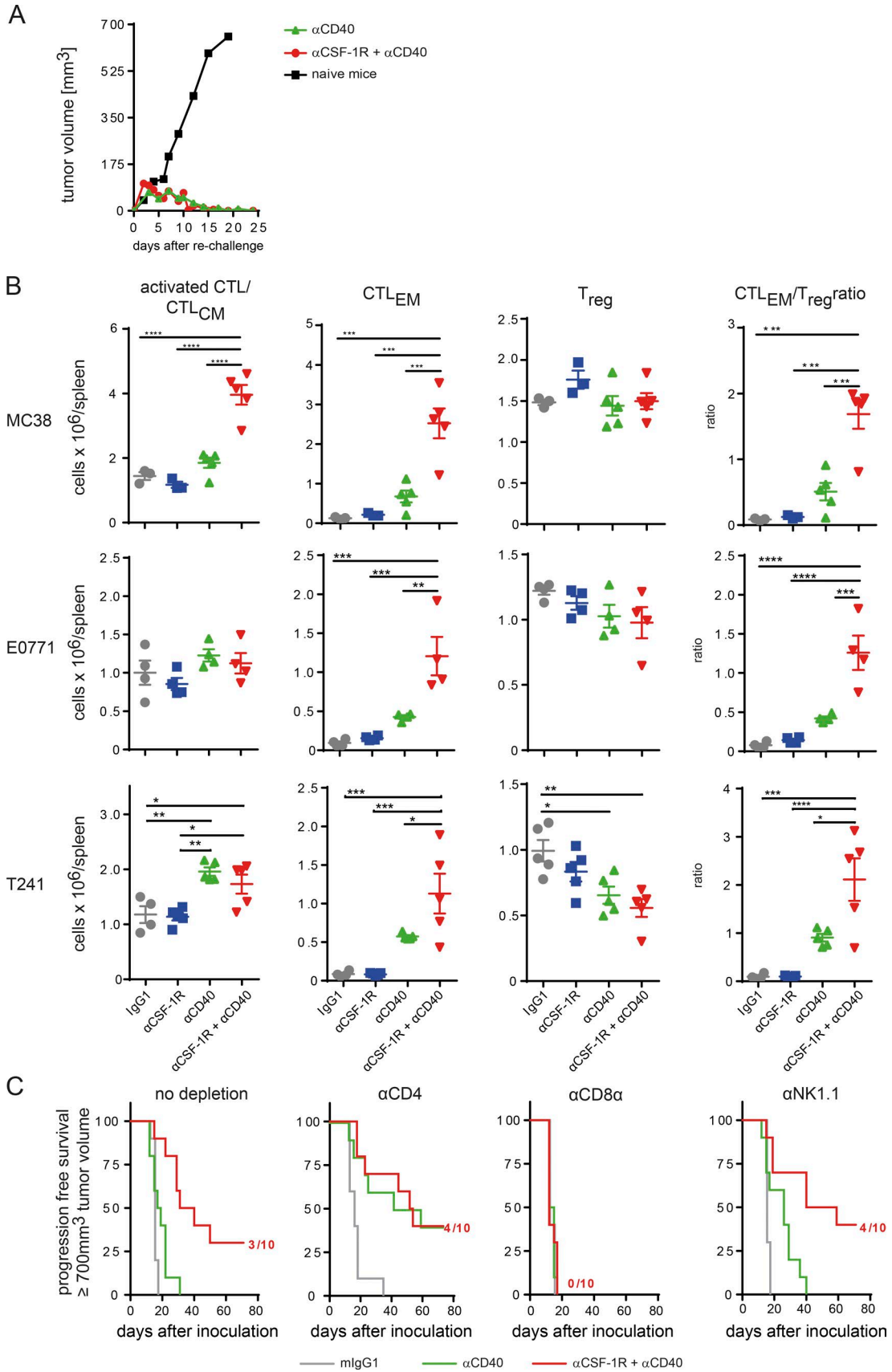
for complete tumor eradication by αCSF-1R+αCD40, also leading to immunological memory.

CD40 is expressed on the TAMs of cancer patients

Our preclinical analysis revealed a strong activation of TAMs by CSF-1R blockade together with CD40 activation and triggered the investigation of CD40 expression on TAMs in patient-derived primary tumors. We analyzed different tumor types that were described as heavily infiltrated by TAMs (Zhang et al., 2012). Therefore, we developed a duplex staining for CD40 together with CD68 in immunohistochemistry (IHC) and included two additional TAM markers (CD163 and CSF-1R) in consecutive sections (Fig. 5 A). Interestingly, we observed a positive correlation of CD40^{+} TAM infiltrates with CD163^{+} TAM and CSF-1R^{+} TAM cell densities in colorectal adenocarcinoma and mesothelioma (Fig. 5 B). Notably, in mesothelioma, the interpatient variability of CD40^{+} TAM densities was more pronounced compared with colorectal cancer (CRC) samples (Fig. 5 C and Table S4). Furthermore, CD3^{+} T cells were found to colocalize with the CSF-1R^{+} TAM infiltrate (Fig. 5 D). Collectively, the IHC analysis of patient tumor tissue revealed that CD40 is expressed on TAM and can vary between individual patients. The differences in CD40^{+} TAM densities and tumor-specific T cells in tumors, alongside a high mutational load, can serve as criteria among others to select tumor types for a clinical trial that evaluates the benefit from αCSF-1R+αCD40 combination therapy in cancer patients.

From a safety perspective, macrophage-mediated TNF-α release may contribute to transient transaminitis observed in patients treated with CD40 agonist (Beatty et al., 2013; Bouchlaka et al., 2013; Byrne et al., 2016). Therefore, the strong reprogramming of macrophages by the αCSF-1R+αCD40 combination in healthy tissue might exacerbate the CD40 agonist–induced cytokine release, for example, in the liver, where the biggest pool of macrophages resides compared to other tissues. To assess the potential toxicity of dual CD40 and CSF-1R targeting, we evaluated body weight changes in treated animals (Fig. S5 A). Monotherapy of αCD40 resulted in a transient decline in body weight, peaking on day 3, that correlated with transient histopathological changes of liver damage, with recovery 9 d after therapy initiation. The combination with αCSF-1R antibody did not show any additional microscopic signs of increased or prolonged liver toxicity compared with αCD40 monotherapy (Fig. S5, B and C).

DISCUSSION

CSF-1R inhibitors have been shown to modulate TAMs and MDSCs in multiple ways, ranging from depletion to reprogramming, as demonstrated in preclinical mouse studies (Zhu et al., 2014; Baer et al., 2016; Holmgaard et al., 2016). Consistent with the T cell suppressive role of myeloid cells, myeloid cell targeting via CSF-1R inhibitors has been combined with T cell–activating therapies such as adoptive transfer of T cells and checkpoint inhibitors (Zhu et al., 2014; Eissler et al., 2016; Holmgaard et al., 2016; Marigo et al., 2016). Most studies reported a favorable antitumor effect for these combinations. However, antitumor T cell responses were reduced in the presence of a CSF-1R small molecule inhibitor that was given before vaccination (van der Sluis et al., 2015). Van der Sluis and colleagues also speculated in this publication that TAM-repolarizing agents might be superior to TAM-depleting therapeutics.

Here, we provide evidence that TAMs can be transiently reprogrammed before αCSF-1R antibody–mediated elimination. This repolarization requires combination with a CD40 agonist, resulting in both rapid TAM activation and subsequently reinvigoration of a preexisting T cell response against the tumor, allowing synergistic antitumoral activity. Our data suggest that the inhibition of CSF-1R signaling acts as an amplifier of CD40 agonist–regulated general immune activation via TAM reprogramming. Notably, the effectiveness of this combination demands the presence of TAMs, as depletion of TAMs before αCSF-1R+αCD40 therapy abrogated the therapeutic benefit completely. At first glance, this combination may appear counterintuitive, as macrophages are depleted by αCSF-1R antibodies but are, however, key mediators of αCD40 antitumoral effects (Vonderheide and Glennie, 2013; Ries et al., 2014; Holmgaard et al., 2016). This conundrum might be explained by the fast activation of CD40-expressing cells together with the slow kinetics of TAM depletion. Our study suggests that the inhibition of CSF-1R signaling reverses the suppression by TAMs faster than the induction of apoptosis within the same cell by blocking its survival signal. TAM transcriptome, whole tumor NanoString, and protein multiplex analyses independently support the notion that

Figure 4. Tumor rejection by αCSF-1R+αCD40 combination depends on CD8^{+} T cells. (A) Rechallenge of tumor-free mice upon αCD40 or αCSF-1R+αCD40 leads to rapid rejection of MC38 tumors. Mice were rechallenged with 5×10^6 MC38 tumor cells into the contralateral flank from the first tumor, and tumor volume was monitored. Data are pooled from four rechallenge experiments (total $n = 5$ naive mice, $n = 7$ αCD40, and $n = 47$ αCSF-1R+αCD40). **(B)** MC38, E0771, and T241 tumor-bearing mice were treated with mIgG1 weekly, αCSF-1R weekly, αCD40 once, or αCSF-1R weekly + αCD40 once, and splenocytes were analyzed on day 10. CD8^{+} T cells were analyzed for effector memory status (CTL$_{EM}$) or activated/central memory (activated CTL/CTL$_{CM}$), and the number of FoxP3^{+} T reg cells was assessed by flow cytometry. Graphs show means ± SEM, statistical analysis by one-way ANOVA, and Tukey correction with $n = 3$ to 5 per group as depicted from one out of a minimum of two independent experiments. **(C)** Rejection of MC38 tumors is mediated by CD8^{+} T cells. MC38 tumor-bearing animals were treated with depletion antibodies against CD4^{+}, CD8^{+} T cells, or NK cells starting on days −3 and −1 before therapy with mIgG1, αCD40, or αCSF-1R+αCD40 on day 0. An additional three doses of depleting antibodies were given at days 1, 4, and 7. Mice were graphically censored once the tumor sized reached ≥700 mm³, and numbers in graphs indicate amount of tumor-free mice within the specific group ($n = 10$ for all groups depicted). Data depicted are exemplary from two independent experiments. *, $P < 0.05$; **, $P < 0.01$; ***, $P < 0.001$; ****, $P < 0.0001$.
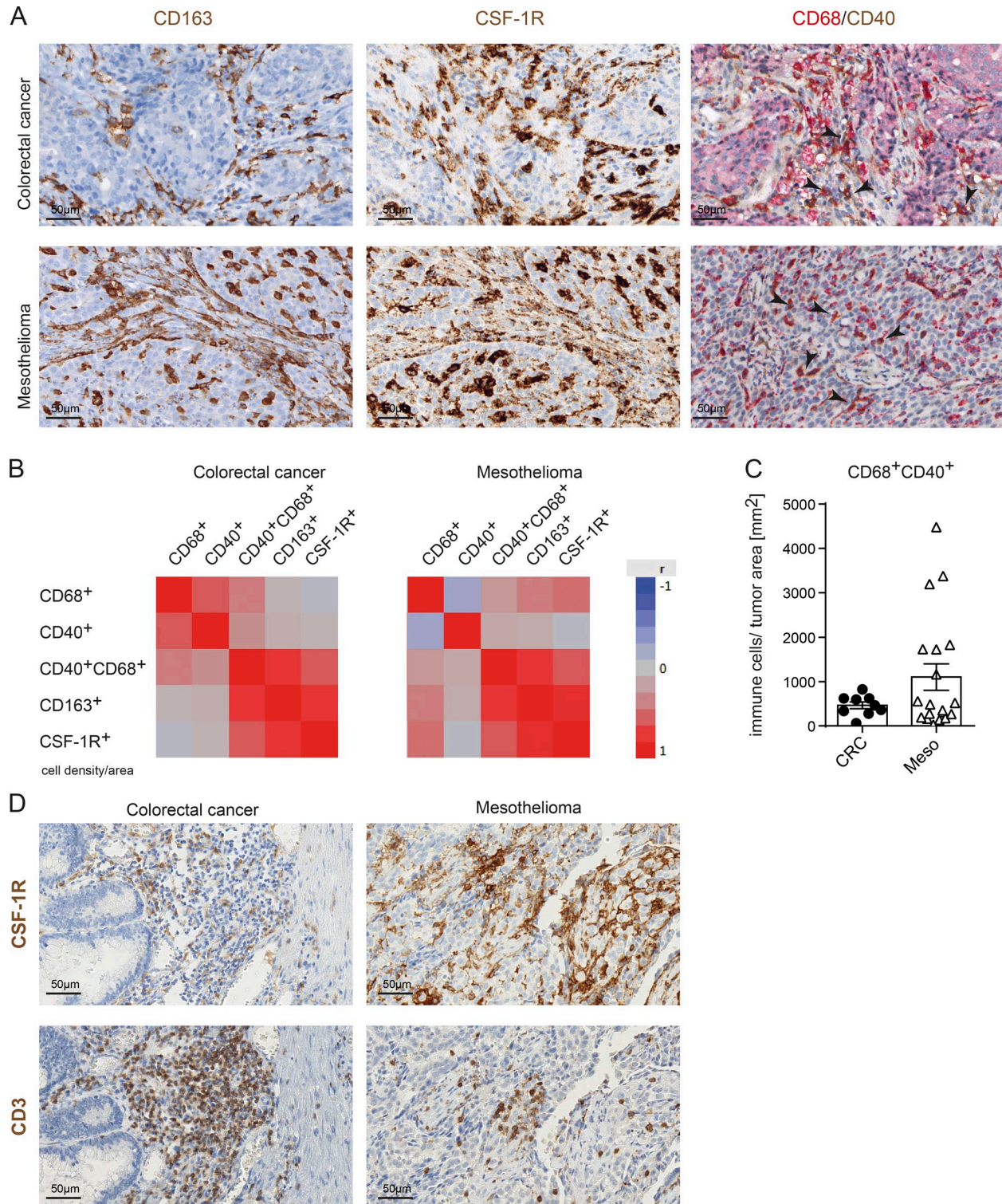
Figure 5. **CD40 is expressed on TAMs of cancer patients. (A)** Exemplary IHC images for CD163 and CSF-1R staining and duplex staining for CD68/CD40 staining of one exemplary CRC and one exemplary mesothelioma patient. Black arrowheads indicate examples of CD68⁺CD40⁺ double-positive macrophages. **(B)** Overall correlation shown as heat maps of 9 CRC and 19 mesothelioma patients using data obtained by automated digital analyses. **(C)** CD68⁺CD40⁺ double-positive cells in CRC and mesothelioma patients quantified as cell counts per squared millimeters of tumor tissue by digital analyses. **(D)** CSF-1R⁺ macrophages and CD3⁺ T cells colocalize in CRC and mesothelioma as assessed from consecutive sections.

dual αCSF-1R+αCD40 targeting promotes a proinflammatory TAM phenotype associated with augmented inflammatory cytokine (IL-1β and IL-27) and chemokine (CCL2 and CCL5) production. However, the exact nature of the myeloid populations responsive to the combination remains elusive. A detailed kinetic transcriptome analysis would be needed to differentiate whether preexisting TAMs, in situ differentiated TAMs from repopulating MDSCs, or TAMs originating from the spleen represent the effector cell population in this combination. Given the profound changes that were detectable 16 h after therapy initiation, it is conceivable that preexisting TAMs are involved. Nevertheless, our study clearly shows that the combination does not protect TAMs from αCSF-1R–mediated depletion, as TAM depletion was comparable in all αCSF-1R–treated groups.

Interestingly, the strong αCSF-1R+αCD40-induced TAM activation may also override the T reg cell–mediated counter-regulating effects induced by the CD40 agonist alone. The strongest regulated gene detected was the CCR4^{+} T reg or CCR4^{+} NK cell recruiting chemokine CCL22 upon αCSF-1R+αCD40 combination when compared with αCD40 monotherapy (Scheu et al., 2017). Interestingly, NK cell depletion had no effect, but depletion of CD4^{+} T cells even enhanced the antitumoral effect of the single agent αCD40, but not of the αCSF-1R+αCD40 combination, suggesting an additional regulation of the T reg cell–suppressive phenotype by the proinflammatory tumor microenvironment (Fig. 4 C; Guiducci et al., 2005; Jenabian et al., 2014). Furthermore, dual CSF-1R and CD40 targeting increased the expression of IL-27, which plays an important role in suppressing the development and function of T reg cells. It is tempting to speculate that IL-27 is not only involved in maintaining the Th1 response but also in tempering the counteracting T reg cell activation (Wang and Liu, 2016).

Dual CSF-1R and CD40 targeting was evaluated in two other independent studies that used either a CSF-1R small molecule or different antibody in a transplanted and a genetically engineered mouse model equipped with heterogeneous myeloid cell composition (see Perry et al. in this issue; Wiehagen et al., 2017). The study by Wiehagen et al. (2017) emphasizes the role of CD40 agonist in DC activation in concert with CSF-1R inhibition on TAMs. On the contrary, our investigations and the work from Perry et al. (2018) unravel the synergizing combination effects on TAMs in creating a unique, highly inflammatory TAM phenotype (Perry et al., 2018). Despite the differences in the degree of elimination efficacy of suppressive TAMs, inflammatory TAM differentiation, or reprogramming, which might be attributed to the models or CSF-1R inhibitors used, all studies concur in demonstrating a T cell–dependent enhanced antitumoral effect for this combination. The pleiotropic activity of the CD40 agonist, which not only targets multiple cell types but also triggers the release of an array of factors from each activated cell, may account for the observed differential skewing of the plastic, specifically tumor-shaped myeloid infiltrate.

Nonetheless, the combination effects on the various myeloid cell types are potent enough to promote an adaptive immune response against a broad range of tumors.

The pleiotropic CD40 agonist function leads us to speculate that other pharmacological strategies pursuing TAM targeting may also benefit from this combination partner (Mantovani et al., 2017). Particularly, CD47/SIRPα inhibitors might equally synergize in TAM hyperactivation in combination with αCD40, as stimulation of phagocytosis may provide the necessary second activation signal. In contrast, approaches that interfere with TAM recruiting by, e.g., blocking the CCL2 chemokine are less likely to synergize with CD40 agonist as a result of the lack of direct activating or reduced inhibitory signals on TAMs.

The finding that the αCSF-1R+αCD40 combination transiently triggers a potent hyperactivated TAM phenotype has important implications for clinical development with regard to (a) dosing schedule, (b) safety, and (c) further combination with checkpoint blockade inhibitors. The antibodies are normally administered to patients in regular cycles, and therefore, TAMs would only be present during the first but not the following cycles using continuous exposure to αCSF-1R. To achieve the maximum benefit from transient TAM reprogramming, a less frequent dosing of αCSF-1R may be warranted to allow TAM recovery and subsequently repeated activation (Fig. 6). Indeed, this concept of transient TAM depletion is currently being evaluated in an early clinical trial using emactuzumab and RO7009789 (ClinicalTrials.gov identifier NCT02760797). Unfortunately, an intermittent treatment schedule is not feasible in mouse models. Using long treatment intervals that are needed for complete TAM recovery is severely compromised by anti–drug antibody formation against the rat anti–mouse CD40 antibody clone FGK.45 used in the present study (Beatty et al., 2011).

From a safety perspective, macrophage-derived TNF-α may contribute to the transient transaminitis observed in patients treated with αCD40 (Beatty et al., 2013). Importantly, our preclinical studies in mice did not reveal any additional signs of increased liver toxicity for the combination, compared with αCD40 monotherapy (Fig. S5). The relatively broad expression profile of CD40 including platelets and endothelial cells is another aspect for consideration. Though CSF-1R is not coexpressed on these cell types (Stanley and Chitu, 2014), perivascular macrophages were depleted in non–tumor-bearing mice by CSF-1R inhibitors and shown to interact with the vascular endothelium (He et al., 2016). Hence, alterations in vessel integrity under conditions of perivascular TAM depletion by CSF-1R blockade and endothelial cell or platelet activation by the CD40 agonist cannot be excluded.

Lastly, the aspect of patient selection for this novel combination needs to be taken into account. The findings of this study offer new insights on the criteria to use for selection of tumor types that are more likely to respond to this particular therapy. These criteria include frequency of CD40^{+} TAM infiltrate, colocalization of CD40^{+} TAMs with T cells,

870

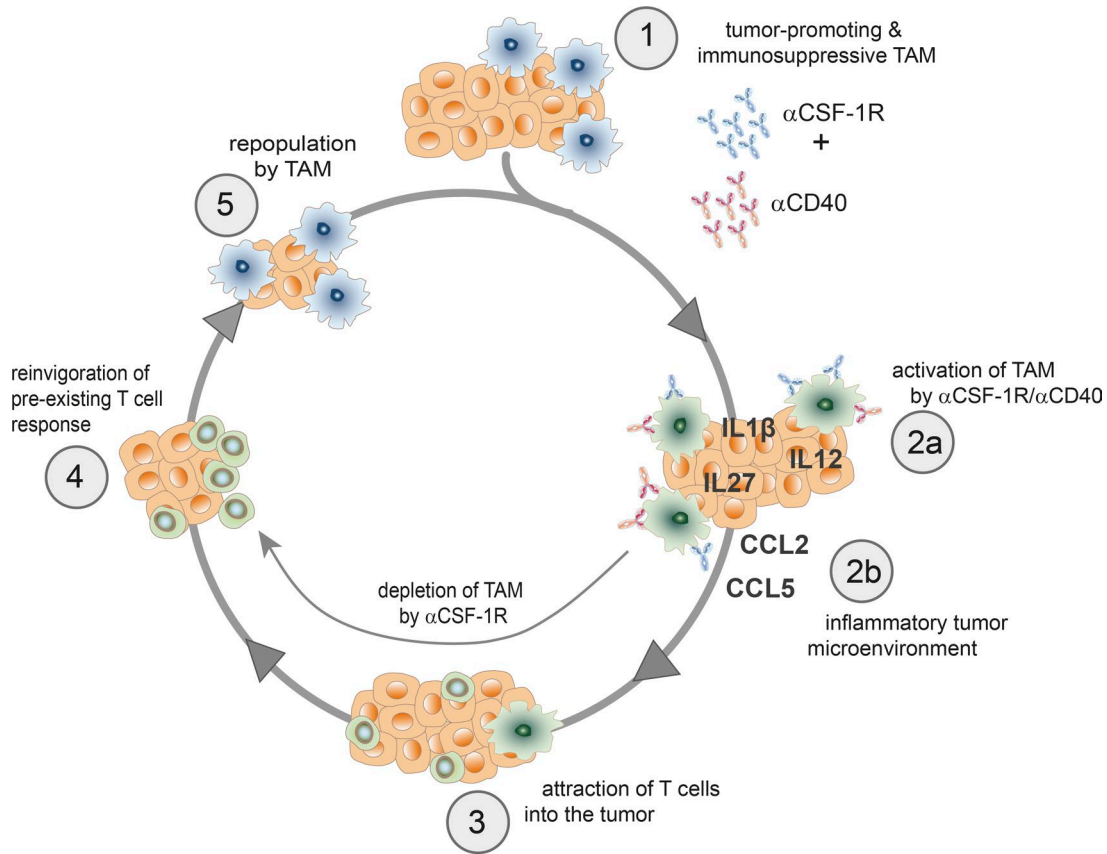Short-term TAM hyperactivation by anti–CSF-1R+CD40 | Hoves et al.

Figure 6. **Schematic representation of the potential mechanism using short–term activated TAMs to reinvigorate a preexisting T cell response.**

and acquired resistance to immune checkpoint inhibition. Because our data demonstrate an up-regulation of the PD-L1 mRNA level in the tumor microenvironment induced by αCSF-1R+αCD40, even a triple combination with check-point inhibitors has scientific merit, provided that a tolerable safety profile can be achieved. Collectively, our observations provide a novel mechanism to redirect TAMs against the tumor that is currently translated to the clinic to evaluate whether the dual targeting of CSF-1R+CD40 is able to drive effective antitumor immunity not only in mice but also in patients.

MATERIALS AND METHODS
Mouse studies
Female C57BL/6N or BALB/c mice (6–8 wk of age; Charles River Laboratory) were inoculated with the respective tumor cell lines. The adenocarcinoma cell line MC38, the sarcoma cell line T241, and the colon cancer cell line CT26.WT were inoculated s.c. (all 10^6 per mouse). The breast cancer cell line E0771 (2.5×10^5) was inoculated into the mammary fad pad. All cell lines were confirmed to be free of mycoplasma and murine viruses by PCR testing (Charles River Laboratory). All commercially obtained and in–house–generated antibodies as well as the dilution buffer (20 mM histidine and 140 mM NaCl, pH 6.0) were endotoxin free by limulus amebocyte lysate test.

Tumor growth curves were monitored by caliper measurement. Animals were graphically censored in Kaplan–Meier curves once they reached ≥ 700 mm^3. However, tumor volumes were collected regularly until termination criteria were reached according to the National Institutes of Health Guidelines for the Care and Use of Laboratory Animals and European Union directives and guidelines. All procedures were performed according to the approvals by the Regierung Oberbayern.

For the OT-I priming experiment, C57BL/6N, C57BL/6OT-I, and C57BL/6 CD45.1 mice were purchased from Charles River Laboratory. C57BL/6 OT-I mice were crossed with C57BL/6 CD45.1 mice to obtain CD45.1–expressing C57BL/6 OT-I mice. C57BL/6 OT-I/CD45.2/ CD45.1 and C57BL/6 OT-I/CD45.1 mice were maintained as colonies at École Polytechnique Fédérale de Lausanne. The MC38-OVA cell line was provided by Nicole Haynes (Peter MacCallum Cancer Center, Melbourne, Australia). All procedures were performed according to protocols approved by the Veterinary Authorities of the Canton Vaud, Switzerland, according to the Swiss Law (3046).

In vivo αCSF–1R and αCD40 combination
10 mice per group were treated with 30 mg/kg murine IgG1 isotype control (clone MOPC–21; BioXCell) and 4 mg/kg

rat IgG2a isotype control (clone 2A3; BioXCell), 30 mg/kg anti–CSF-1R antibody (clone 2G2; Ries et al., 2014), 4 mg/kg αCD40 antibody (rat IgG2a clone FGK.45; BioXCell), or the combination of both targeting antibodies. αCD40 or the matching isotype control was only administered once, whereas αCSF-1R antibody was administered weekly unless otherwise stated (maximum four times total). All antibodies were administered i.p. unless otherwise stated.

In vivo sequencing experiment

Mice were inoculated with MC38 tumor cells and were allocated to groups for starting αCSF-1R treatment ∼80 mm^3 (day 7) or ∼200 mm^3 (day 11). Only αCD40 treatment was sequenced (a) concomitant with αCSF-1R (αCD40+αCSF-1R), (b) 2 d ahead of αCSF-1R (αCD40>αCSF-1R), or (c) 2 d after αCSF-1R treatment (αCSF-1R>αCD40). Final group sizes for testing the altered sequencing were 10 matching tumor volumes at the time of αCSF-1R treatment. Mice were treated with αCSF-1R weekly up to four times total, whereas αCD40 was only administered once as indicated and dosing as described above.

In vivo αPD-1 and αPD-1+αCTLA-4 treatment

αPD-1 (clone RPMI1-14), αCTLA-4 (clone 9D9), and the isotype antibody rat IgG2a (clone 2A3) were obtained from BioXCell. Animals were inoculated with MC38 tumor cells, and treatment started at the indicated tumor sizes. 10 mg/kg αPD-1 and 4 mg/kg αCTLA-4 were given three times every 3 d.

In vivo macrophage depletion

Mice were inoculated with MC38 tumor cells and treated with 30 mg/kg murine IgG1, IgG1-FcØ, or αCSF-1R–FcØ on days 3 and 9 after inoculation. The FcγR-incompetent version comprised a human IgG1 backbone carrying the LALA-P329G mutation, not allowing binding to both human and mouse FcγR. Depletion of TAM was confirmed by flow cytometry on day 11. Animals received a single, simultaneous dose of 4 mg/kg αCD40 and 30 mg/kg αCSF-1R on day 11 when tumor size reached 190 mm^3. One group that was pretreated by IgG1-FcØ received a single, simultaneous dose of 30 mg/kg αCD40+αCSF-1R–FcØ.

In vivo OT-1 priming

After isolation, OT-1 T cells were stained with the CellTrace violet cell proliferation kit (Molecular Probes) according to the manufacturer's protocol before injection into the mice. In brief, cells were resuspended in PBS, diluted 1:1,000 in CellTrace violet, incubated for 30 min on 4°C, and subsequently washed in FACS buffer (PBS and 2% FBS). Animals received 10^7 labeled OT-1 cells when tumors reached a size of 100 mm^3. On the next day, mice were treated with αCSF-1R+αCD40 antibodies or the matching controls. The transferred OT-1 cells were analyzed on day 3 by flow cytometry from spleens.

In vivo lymphocyte depletion

To deplete CD4$^+$ and CD8$^+$ T cells as well as NK cells, mice were treated on days −3 and −1, before administration of therapeutic antibodies (day 0) and on days 1, 4, and 7 thereafter with 100 μg/mouse of depleting antibodies (mouse anti-CD4 antibody, clone GK1.5, BioLegend; anti-NK1.1 antibody, clone PK136, BioXCell; and anti-CD8α antibody, clone 53–6.7, BioXCell). Animals that only were treated with the depleting antibodies were injected with saline equal in volume to αCD40±αCSF-1R antibodies. All antibodies were given i.p.

Eye and tumor imaging studies

Female BALB/c mice were inoculated s.c. with 10^6 CT-26. WT. At 100 mm^3 in mean, groups were allocated for antibody treatment. The therapeutic αCD40 rat IgG2a antibody clone FGK.45 (BioXCell) was labeled in-house using Alexa Fluor 647 dye (αCD40-AF647) by cross-linking monoreactive N-hydroxysuccinimide ester and lysine residues according to the manufacturer's instructions (Thermo Fisher). The antibody was purified by dialysis and size-exclusion chromatography, and subsequently, binding characteristics of αCD40-AF647 were confirmed by surface plasmon resonance analysis. No significant changes were detected in the kinetics constants (K$_{on}$/K$_{off}$) between labeled and unlabeled antibody variants.

Six mice per group were treated with 4 mg/kg αCD40-AF647 under isoflurane inhalation anesthesia i.v., i.p., or s.c. via a 26-G catheter. Fluorescence signal intensities of αCD40-AF647 were monitored and analyzed using the MAESTRO imaging system (PerkinElmer). Eye imaging was started 10 s before antibody administration and performed with a rate of four frames per minute over a continuous 20-min time period with automatically adapted exposure times (excitation filter, 615–665 nm; emission filter, 700-nm long pass). Subsequently, fluorescence signal intensities were monitored at indicated time points after mAb administration (1, 4, 7, 24, and 48 h) in the eye and tumor region. All acquired image cubes were spectrally unmixed and quantified in regions of interest over the eye or the tumor, respectively. The signal intensity of the first image from before antibody administration was defined as zero point/background fluorescence. The acquired fluorescence intensities from eye and tumor regions of interest were plotted over time.

Flow cytometry analysis

Tumors, spleens, or blood samples were taken at the time points indicated in the figure legends. Tumors were excised, and single-cell suspensions were obtained by mechanical processing and enzymatical digestion (0.01% DNase, 1 mg/ml dispase, and 1 mg/ml collagenase IV). Spleens were mechanically processed and stained upon erythrocyte lysis (Roche). For analysis of peripheral blood leukocytes, 25 μl of whole blood collected in EDTA-coated tubes (Sarstedt) was analyzed after red cell lysis. Quantification was performed using blank sphero beads (BD Bioscience) during acquisition. All

staining procedures started with Fc receptor blocking using the 2.4G2 antibody clone (BD Bioscience), and the following antibodies (clones) were used to analyzed leukocyte infiltrate: CD45 (30-F11), CD11b (M1/70), F4/80 (BM8), Ly6G (1A8), Ly6C (AL-21), NK1.1 (PK136), CD4 (RM4-5), CD8 (53-6.7), CD19 (6D5), CD24 (M1/69), CD40 (1C10) CD44 (IM7), CD62L (MEL-14), CD69 (H1.2F3), CD103 (2E7), CD274 (10F.9G2), MHC class II I-A/I-E (M5/114.15.2), and the matching isotype controls, all from BioLegend or BD Bioscience; CD45.2 (104) and CD45.1 (A20) from eBioscience; and CD8 (5H10) for the OT-1 study from Invitrogen. Intracellular FoxP3 (clone FJK-16s) staining was performed according to the manufacturer's instructions (complete kit; eBioscience). Viability was determined using either DAPI or fixable Zombie Aqua dyes (BioLegend). Data were acquired on BD Bioscience FACSCanto II, LSR II, or LSRFortessa machines and finally analyzed using FlowJo software version 10. The populations shown were defined as follows, succeeding viability and single-cell gating: total leukocytes as $CD45^+$; myeloid cells as $CD45^+/CD11b^+$; TAMs as $CD45^+CD11b^+F4/80^{high}Ly6C^{low}Ly6G^{negative}$; total MDSCs as $CD45^+CD11b^+F4/80^{low}$; $Ly6C^{low}$ MDSC/TAM precursors as $CD45^+CD11b^+F4/80^{low}Ly6C^{low}$; monocytic MDSCs as $CD45^+CD11b^+F4/80^{low}Ly6C^{high}Ly6G^{negative}$; granulocytic MDSCs as $CD45^+CD11b^+F4/80^{low}Ly6C^{low}Ly6G^{high}$; total lymphoid cells as $CD45^+/CD11b^-$; NK cells (tumor) as $CD45^+NK1.1^+$; $CD8^+$ T cells as $CD45^+CD11b^-CD8\alpha^+$; $CD4^+$ T cells as $CD45^+CD11b^-CD4^+$; and T reg cells as $CD45^+CD11b^-CD4^+FoxP3^+$. For DC analysis from tumors, total DCs were defined as $CD45^+CD11b^+Ly6C^{negtive}Ly6G^{negative}$ MHC class $II^{high}F4/80^{low}CD24^{positive}$, and migratory DCs (DC2) also were found to be $CD103^{positive}$, whereas DC1 was $CD11b^{positive}$. Spleen DCs were defined as $CD45^+CD11c^{high}CD8\alpha^+$ (cross-presenting DCs) or $CD8\alpha^-$ (comprising the $CD4^+$ and $CD4^+CD8^+$ double-negative DC populations).

RNA sequencing and computational signature analysis

RNA sequencing of sorted myeloid cell populations was performed as recently described (Sandmann et al., 2014; Baer et al., 2016). Signature analysis of gene expression values by a publicly available tool resulted in Wilcoxon/Mann-Whitney rank sum statistics, representing the activation level or likelihood level of the pathway or phenotype represented by a signature in a treatment group compared with another. Three comparisons were performed for each treatment group; e.g., the combination of $\alpha CSF-1R+\alpha CD40$ was compared separately against the $\alpha CD40$, $\alpha CSF-1R$, and IgG isotype control groups. A total of 88 signatures obtained from the Molecular Signatures Database of perturbations of various cell types (e.g., immune cells, cancer cells, and mammary epithelial cells), involving LPS, IFN, or TNF stimulation and three M1/M2 signatures, were used to check for general immune activation effects (Subramanian et al., 2005; Schmieder et al., 2012; Martinez et al., 2013). RNA sequencing data were submitted to the GEO repository under the accession no. GSE99808.

NanoString and computational analysis

Total RNA was isolated from fresh-frozen mouse tumor tissues taken 16 h after the start of treatment and homogenized in RNA lysis buffer followed by RNEasy Mini kit (Qiagen). Gene expression was quantified with the NanoString nCounter platform using 200 ng of total RNA in the nCounter Mouse Immunology Panel, comprising 561 immunology-related mouse genes (NanoString Technologies). The code set was hybridized with the RNA overnight at 65°C. RNA transcripts were immobilized and counted using the NanoString nCounter Digital Analyzer. Normalized raw expression data (nSolver Analysis) were analyzed when two SDs above the geometric mean of the codeset-internal negative control probes were reached. Genes were excluded from further analysis if 90% of their expression was below the background threshold. The 457 genes that remained after background filtering were normalized to the geometric mean of the internal positive controls as well as to four housekeeping genes (*Ppia*, *Eef1g*, *Sdha*, and *Polr2a*).

Protein detection

To determine intratumoral cytokines and chemokines, tumors were harvested 16 h after the start of treatment, snap frozen in LN_2, and stored for future use at −80°C. Tumor lysates were prepared using lysis buffer (Biorad) including factor 1, factor 2, and PMSF using Peqlab Cryolys tissue homogenizer in Precellys ceramic kit tubes with 1.4-mm beads. Protein levels were adjusted after quantification using a bicinchoninic acid protein assay kit (Thermo Fisher) to 10 mg/ml. Cytokines and chemokines were determined using a multiplex Bio-Plex Pro kit (mouse chemokine panel 33-plex and cytokine 23-plex; Biorad) or by ELISA for mouse IL-27 (Invitrogen). Readout was performed using BioPlex 200 (Biorad) or Synergy 2 (BioTek) instruments, respectively.

PK analysis of the $\alpha CSF-1R$ antibody clone 2G2 was performed by an in-house–made ELISA. In brief, biotinylated murine CSF-1R (Sino Biologicals) was coated onto streptavidin-coated plates (Roche) and incubated with mouse sera or purified 2G2 clone for standardization. Bound 2G2 antibody was detected by a peroxidase-conjugated goat anti-mIgG, specific for Fcγ subclass 1 (Jackson), and ABTS (Roche) using a Sunrise reader (Tecan).

IHC tissue analysis

Human tissue samples were obtained from Asterand and Indivumed after informed consent according the supplier's review boards. IHC protocols for CD40/CD68, CSF-1R CD163, and CD3 were performed using 2.5 µm formalin-fixed, paraffin-embedded tissue sections on the BenchMark XT automated stainer with the NEXES version 10.6 software and the UltraView (CD40, CSF-1R, and CD3), OptiView DAB (CD163), or AP red (CD68) detection kits. All reagents except the CD40 (E3704; Spring Bioscience) and CSF-1R (clone 29; Roche) antibodies were obtained from Ventana Medical Systems. Stained slides were subjected to a visual

assessment by a board-certified pathologist (S. Romagnoli), scanned at 20× using the iScan high throughput (Ventana) for automated digital analyses (Chen and Srinivas, 2015).

We developed algorithms to detect and quantify CD68^{+}, CD163^{+}, CSF-1R, and CD40^{+}/CD68^{+} macrophage populations in tissue. To this end, scanned images were processed to obtain single stain channel images to separate the specific staining of the biomarker from that of hematoxylin, followed by the detection and identification of objects of interest. The detected objects were then used to compute the area of coverage into a final readout for the whole tissue section (Table S4).

Statistical analyses

Statistical analysis was performed using Prism version 6 (GraphPad). The statistical tests used are indicated in the figure legends of the individual experiments.

Online supplemental material

Supplemental material associated with this study includes individual tumor growth curves (Fig. S1), a comparison of different routes of CD40 agonist administration (Fig. S2), a FACS characterization of MC38 tumor–infiltrating immune cells including gating strategy (Fig. S3), NanoString RNA expression values of immune markers and flow cytometry analysis of MC38-OVA tumor immune cell infiltrate (Fig. S4), and body weight curves and liver histology (Fig. S5). Supplemental tables include a comparison of RNA sequencing with published signatures (Table S1), statistical analyses of tumor growth (Table S2), comparison of whole tumor NanoString and isolated TAM RNA sequencing expression data (Table S3), and quantification of IHC stainings on patient tumor samples (Table S4).

REFERENCES

Baer, C., M.L. Squadrito, D. Laoui, D. Thompson, S.K. Hansen, A. Kiialainen, S. Hoves, C.H. Ries, C.H. Ooi, and M. De Palma. 2016. Suppression of microRNA activity amplifies IFN-γ-induced macrophage activation and promotes anti-tumour immunity. *Nat. Cell Biol.* 18:790–802. https://doi.org/10.1038/ncb3371

Beatty, G.L., E.G. Chiorean, M.P. Fishman, B. Saboury, U.R. Teitelbaum, W. Sun, R.D. Huhn, W. Song, D. Li, L.L. Sharp, et al. 2011. CD40 agonists alter tumor stroma and show efficacy against pancreatic carcinoma in mice and humans. *Science.* 331:1612–1616. https://doi.org/10.1126/science.1198443

Beatty, G.L., D.A. Torigian, E.G. Chiorean, B. Saboury, A. Brothers, A. Alavi, A.B. Troxel, W. Sun, U.R. Teitelbaum, R.H. Vonderheide, and P.J. O'Dwyer. 2013. A phase I study of an agonist CD40 monoclonal antibody (CP-870,893) in combination with gemcitabine in patients with advanced pancreatic ductal adenocarcinoma. *Clin. Cancer Res.* 19:6286–6295. https://doi.org/10.1158/1078-0432.CCR-13-1320

Biswas, S.K., and A. Mantovani. 2010. Macrophage plasticity and interaction with lymphocyte subsets: cancer as a paradigm. *Nat. Immunol.* 11:889–896. https://doi.org/10.1038/ni.1937

Bouchlaka, M.N., G.D. Sckisel, M. Chen, A. Mirsoian, A.E. Zamora, E. Maverakis, D.E. Wilkins, K.L. Alderson, H.H. Hsiao, J.M. Weiss, et al. 2013. Aging predisposes to acute inflammatory induced pathology after tumor immunotherapy. *J. Exp. Med.* 210:2223–2237. https://doi.org/10.1084/jem.20131219

Bovenschen, N., and J.A. Kummer. 2010. Orphan granzymes find a home. *Immunol. Rev.* 235:117–127. https://doi.org/10.1111/j.0105-2896.2010.00889.x

Buhtoiarov, I.N., H.D. Lum, G. Berke, P.M. Sondel, and A.L. Rakhmilevich. 2006. Synergistic activation of macrophages via CD40 and TLR9 results in T cell independent antitumor effects. *J. Immunol.* 176:309–318. https://doi.org/10.4049/jimmunol.176.1.309

Byrne, K.T., N.H. Leisenring, D.L. Bajor, and R.H. Vonderheide. 2016. CSF-1R–Dependent Lethal Hepatotoxicity When Agonistic CD40 Antibody Is Given before but Not after Chemotherapy. *J. Immunol.* 197:179–187. https://doi.org/10.4049/jimmunol.1600146

Chen, T., and C. Srinivas. 2015. Group sparsity model for stain unmixing in brightfield multiplex immunohistochemistry images. *Comput. Med. Imaging Graph.* 46:30–39. https://doi.org/10.1016/j.compmedimag.2015.04.001

Coussens, L.M., L. Zitvogel, and A.K. Palucka. 2013. Neutralizing tumor-promoting chronic inflammation: a magic bullet? *Science.* 339:286–291. https://doi.org/10.1126/science.1232227

Dahan, R., B.C. Barnhart, F. Li, A.P. Yamniuk, A.J. Korman, and J.V. Ravetch. 2016. Therapeutic Activity of Agonistic, Human Anti-CD40 Monoclonal Antibodies Requires Selective FcγR Engagement. *Cancer Cell.* 29:820–831. https://doi.org/10.1016/j.ccell.2016.05.001

De Henau, O., M. Rausch, D. Winkler, L.F. Campesato, C. Liu, D.H. Cymerman, S. Budhu, A. Ghosh, M. Pink, J. Tchaicha, et al. 2016. Overcoming resistance to checkpoint blockade therapy by targeting PI3Kγ in myeloid cells. *Nature.* 539:443–447. https://doi.org/10.1038/nature20554

Eissler, N., Y. Mao, D. Brodin, P. Reuterswärd, H. Andersson Svahn, J.I. Johnsen, R. Kiessling, and P. Kogner. 2016. Regulation of myeloid cells by activated T cells determines the efficacy of PD-1 blockade.

OncoImmunology. 5:e1232222. https://doi.org/10.1080/2162402X.2016.1232222

Elgueta, R., M.J. Benson, V.C. de Vries, A. Wasiuk, Y. Guo, and R.J. Noelle. 2009. Molecular mechanism and function of CD40/CD40L engagement in the immune system. *Immunol. Rev.* 229:152–172. https://doi.org/10.1111/j.1600-065X.2009.00782.x

Eliopoulos, A.G., and L.S. Young. 2004. The role of the CD40 pathway in the pathogenesis and treatment of cancer. *Curr. Opin. Pharmacol.* 4:360–367. https://doi.org/10.1016/j.coph.2004.02.008

Fonsatti, E., M. Maio, M. Altomonte, and P. Hersey. 2010. Biology and clinical applications of CD40 in cancer treatment. *Semin. Oncol.* 37:517–523. https://doi.org/10.1053/j.seminoncol.2010.09.002

Gajewski, T.F., H. Schreiber, and Y.X. Fu. 2013. Innate and adaptive immune cells in the tumor microenvironment. *Nat. Immunol.* 14:1014–1022. https://doi.org/10.1038/ni.2703

Gentleman, R., and R. Ihaka. 2017. The R Stats Package. Documentation for package 'stats' version 3.5.0. https://stat.ethz.ch/R-manual/R-devel/library/stats/html/00Index.html

Gordon, S., and F.O. Martinez. 2010. Alternative activation of macrophages: mechanism and functions. *Immunity.* 32:593–604. https://doi.org/10.1016/j.immuni.2010.05.007

Grewal, I.S., and R.A. Flavell. 1998. CD40 and CD154 in cell-mediated immunity. *Annu. Rev. Immunol.* 16:111–135. https://doi.org/10.1146/annurev.immunol.16.1.111

Guiducci, C., A.P. Vicari, S. Sangaletti, G. Trinchieri, and M.P. Colombo. 2005. Redirecting in vivo elicited tumor infiltrating macrophages and dendritic cells towards tumor rejection. *Cancer Res.* 65:3437–3446. https://doi.org/10.1158/0008-5472.CAN-04-4262

He, H., J.J. Mack, E. Güç, C.M. Warren, M.L. Squadrito, W.W. Kilarski, C. Baer, R.D. Freshman, A.I. McDonald, S. Ziyad, et al. 2016. Perivascular Macrophages Limit Permeability. *Arterioscler. Thromb. Vasc. Biol.* 36:2203–2212. https://doi.org/10.1161/ATVBAHA.116.307592

Herbst, R.S., J.C. Soria, M. Kowanetz, G.D. Fine, O. Hamid, M.S. Gordon, J.A. Sosman, D.F. McDermott, J.D. Powderly, S.N. Gettinger, et al. 2014. Predictive correlates of response to the anti-PD-L1 antibody MPDL3280A in cancer patients. *Nature.* 515:563–567. https://doi.org/10.1038/nature14011

Hodi, F.S., S.J. O'Day, D.F. McDermott, R.W. Weber, J.A. Sosman, J.B. Haanen, R. Gonzalez, C. Robert, D. Schadendorf, J.C. Hassel, et al. 2010. Improved survival with ipilimumab in patients with metastatic melanoma. *N. Engl. J. Med.* 363:711–723. https://doi.org/10.1056/NEJMoa1003466

Holmgaard, R.B., A. Brachfeld, B. Gasmi, D.R. Jones, M. Mattar, T. Doman, M. Murphy, D. Schaer, J.D. Wolchok, and T. Merghoub. 2016. Timing of CSF-1/CSF-1R signaling blockade is critical to improving responses to CTLA-4 based immunotherapy. *OncoImmunology.* 5:e1151595. https://doi.org/10.1080/2162402X.2016.1151595

Hu, X., and L.B. Ivashkiv. 2009. Cross-regulation of signaling pathways by interferon-gamma: implications for immune responses and autoimmune diseases. *Immunity.* 31:539–550. https://doi.org/10.1016/j.immuni.2009.09.002

Jenabian, M.A., M. Patel, I. Kema, K. Vyboh, C. Kanagaratham, D. Radzioch, P. Thébault, R. Lapointe, N. Gilmore, P. Ancuta, et al. 2014. Soluble CD40-ligand (sCD40L, sCD154) plays an immunosuppressive role via regulatory T cell expansion in HIV infection. *Clin. Exp. Immunol.* 178:102–111. https://doi.org/10.1111/cei.12396

Kaneda, M.M., K.S. Messer, N. Ralainirina, H. Li, C.J. Leem, S. Gorjestani, G. Woo, A.V. Nguyen, C.C. Figueiredo, P. Foubert, et al. 2016. PI3Kγ is a molecular switch that controls immune suppression. *Nature.* 539:437–442. https://doi.org/10.1038/nature19834

Kulkarni, M.M. 2011. Digital multiplexed gene expression analysis using the NanoString nCounter system. *Curr. Protoc. Mol. Biol.* Chapter 25:10.

Langlais, D., L.B. Barreiro, and P. Gros. 2016. The macrophage IRF8/IRF1 regulome is required for protection against infections and is associated with chronic inflammation. *J. Exp. Med.* 213:585–603. https://doi.org/10.1084/jem.20151764

Li, F., and J.V. Ravetch. 2011. Inhibitory Fcγ receptor engagement drives adjuvant and anti-tumor activities of agonistic CD40 antibodies. *Science.* 333:1030–1034. https://doi.org/10.1126/science.1206954

Lin, E.Y., A.V. Nguyen, R.G. Russell, and J.W. Pollard. 2001. Colony-stimulating factor 1 promotes progression of mammary tumors to malignancy. *J. Exp. Med.* 193:727–740. https://doi.org/10.1084/jem.193.6.727

MacDonald, K.P., J.S. Palmer, S. Cronau, E. Seppanen, S. Olver, N.C. Raffelt, R. Kuns, A.R. Pettit, A. Clouston, B. Wainwright, et al. 2010. An antibody against the colony-stimulating factor 1 receptor depletes the resident subset of monocytes and tissue- and tumor-associated macrophages but does not inhibit inflammation. *Blood.* 116:3955–3963. https://doi.org/10.1182/blood-2010-02-266296

Mantovani, A., F. Marchesi, A. Malesci, L. Laghi, and P. Allavena. 2017. Tumour-associated macrophages as treatment targets in oncology. *Nat. Rev. Clin. Oncol.* 14:399–416. https://doi.org/10.1038/nrclinonc.2016.217

Marigo, I., S. Zilio, G. Desantis, B. Mlecnik, A.H. Agnellini, S. Ugel, M.S. Sasso, J.E. Qualls, F. Kratochvill, P. Zanovello, et al. 2016. T Cell Cancer Therapy Requires CD40-CD40L Activation of Tumor Necrosis Factor and Inducible Nitric-Oxide-Synthase-Producing Dendritic Cells. *Cancer Cell.* 30:651. https://doi.org/10.1016/j.ccell.2016.09.009

Martinez, F.O., S. Gordon, M. Locati, and A. Mantovani. 2006. Transcriptional profiling of the human monocyte-to-macrophage differentiation and polarization: new molecules and patterns of gene expression. *J. Immunol.* 177:7303–7311. https://doi.org/10.4049/jimmunol.177.10.7303

Martinez, F.O., L. Helming, R. Milde, A. Varin, B.N. Melgert, C. Draijer, B. Thomas, M. Fabbri, A. Crawshaw, L.P. Ho, et al. 2013. Genetic programs expressed in resting and IL-4 alternatively activated mouse and human macrophages: similarities and differences. *Blood.* 121:e57–e69. https://doi.org/10.1182/blood-2012-06-436212

Mok, S., R.C. Koya, C. Tsui, J. Xu, L. Robert, L. Wu, T. Graeber, B.L. West, G. Bollag, and A. Ribas. 2014. Inhibition of CSF-1 receptor improves the antitumor efficacy of adoptive cell transfer immunotherapy. *Cancer Res.* 74:153–161. https://doi.org/10.1158/0008-5472.CAN-13-1816

Murphy, T.L., R. Tussiwand, and K.M. Murphy. 2013. Specificity through cooperation: BATF-IRF interactions control immune-regulatory networks. *Nat. Rev. Immunol.* 13:499–509. https://doi.org/10.1038/nri3470

Nakajima, A., T. Kodama, S. Morimoto, M. Azuma, K. Takeda, H. Oshima, S. Yoshino, H. Yagita, and K. Okumura. 1998. Antitumor effect of CD40 ligand: elicitation of local and systemic antitumor responses by IL-12 and B7. *J. Immunol.* 161:1901–1907.

Perry, C.J., A.R. Muñoz-Rojas, K.M. Meeth, L.N. Kellman, R.A. Amezquita, D. Thakral, V.Y. Du, J.X. Wang, W. Damsky, A.L. Kuhlmann, J.W. Sher, et al. 2018. Myeloid-targeted immunotherapies act in synergy to induce inflammation and antitumor immunity. *J. Exp. Med.* https://doi.org/10.1084/jem.20171435

Pyonteck, S.M., L. Akkari, A.J. Schuhmacher, R.L. Bowman, L. Sevenich, D.F. Quail, O.C. Olson, M.L. Quick, J.T. Huse, V. Teijeiro, et al. 2013. CSF-1R inhibition alters macrophage polarization and blocks glioma progression. *Nat. Med.* 19:1264–1272. https://doi.org/10.1038/nm.3337

Rakhmilevich, A.L., K.L. Alderson, and P.M. Sondel. 2012. T-cell-independent antitumor effects of CD40 ligation. *Int. Rev. Immunol.* 31:267–278. https://doi.org/10.3109/08830185.2012.698337

Richman, L.P., and R.H. Vonderheide. 2014. Role of crosslinking for agonistic CD40 monoclonal antibodies as immune therapy of cancer. *Cancer Immunol. Res.* 2:19–26. https://doi.org/10.1158/2326-6066.CIR-13-0152

Ries, C.H., M.A. Cannarile, S. Hoves, J. Benz, K. Wartha, V. Runza, F. Rey-Giraud, L.P. Pradel, F. Feuerhake, I. Klaman, et al. 2014. Targeting tumor-associated macrophages with anti–CSF-1R antibody reveals a strategy for cancer therapy. *Cancer Cell*. 25:846–859. https://doi.org/10.1016/j.ccr.2014.05.016

Ries, C.H., S. Hoves, M.A. Cannarile, and D. Rüttinger. 2015. CSF-1/CSF-1R targeting agents in clinical development for cancer therapy. *Curr. Opin. Pharmacol.* 23:45–51. https://doi.org/10.1016/j.coph.2015.05.008

Rizvi, N.A., M.D. Hellmann, A. Snyder, P. Kvistborg, V. Makarov, J.J. Havel, W. Lee, J. Yuan, P. Wong, T.S. Ho, et al. 2015. Mutational landscape determines sensitivity to PD-1 blockade in non-small cell lung cancer. *Science*. 348:124–128. https://doi.org/10.1126/science.aaa1348

Ruffell, B., and L.M. Coussens. 2015. Macrophages and therapeutic resistance in cancer. *Cancer Cell*. 27:462–472. https://doi.org/10.1016/j.ccell.2015.02.015

Ruffell, B., D. Chang-Strachan, V. Chan, A. Rosenbusch, C.M. Ho, N. Pryer, D. Daniel, E.S. Hwang, H.S. Rugo, and L.M. Coussens. 2014. Macrophage IL-10 blocks CD8+ T cell-dependent responses to chemotherapy by suppressing IL-12 expression in intratumoral dendritic cells. *Cancer Cell*. 26:623–637. https://doi.org/10.1016/j.ccell.2014.09.006

Sandin, L.C., A. Orlova, E. Gustafsson, P. Ellmark, V. Tolmachev, T.H. Tötterman, and S.M. Mangsbo. 2014. Locally delivered CD40 agonist antibody accumulates in secondary lymphoid organs and eradicates experimental disseminated bladder cancer. *Cancer Immunol. Res.* 2:80–90. https://doi.org/10.1158/2326-6066.CIR-13-0067

Sandmann, T., S.K. Kummerfeld, R. Gentleman, and R. Bourgon. 2014. gCMAP: user-friendly connectivity mapping with R. *Bioinformatics*. 30:127–128. https://doi.org/10.1093/bioinformatics/btt592

Scheu, S., S. Ali, C. Ruland, V. Arolt, and J. Alferink. 2017. The C-C Chemokines CCL17 and CCL22 and Their Receptor CCR4 in CNS Autoimmunity. *Int. J. Mol. Sci.* 18:2306. https://doi.org/10.3390/ijms18112306

Schlothauer, T., S. Herter, C.F. Koller, S. Grau-Richards, V. Steinhart, C. Spick, M. Kubbies, C. Klein, P. Umaña, and E. Mössner. 2016. Novel human IgG1 and IgG4 Fc-engineered antibodies with completely abolished immune effector functions. *Protein Eng. Des. Sel.* 29:457–466. https://doi.org/10.1093/protein/gzw040

Schmieder, A., J. Michel, K. Schönhaar, S. Goerdt, and K. Schledzewski. 2012. Differentiation and gene expression profile of tumor-associated macrophages. *Semin. Cancer Biol.* 22:289–297. https://doi.org/10.1016/j.semcancer.2012.02.002

Schroder, K., P.J. Hertzog, T. Ravasi, and D.A. Hume. 2004. Interferon-gamma: an overview of signals, mechanisms and functions. *J. Leukoc. Biol.* 75:163–189. https://doi.org/10.1189/jlb.0603252

Sharma, P., and J.P. Allison. 2015. Immune checkpoint targeting in cancer therapy: toward combination strategies with curative potential. *Cell*. 161:205–214. https://doi.org/10.1016/j.cell.2015.03.030

Singh-Jasuja, H., A. Thiolat, M. Ribon, M.C. Boissier, N. Bessis, H.G. Rammensee, and P. Decker. 2013. The mouse dendritic cell marker CD11c is down-regulated upon cell activation through Toll-like receptor triggering. *Immunobiology*. 218:28–39. https://doi.org/10.1016/j.imbio.2012.01.021

Stanley, E.R., and V. Chitu. 2014. CSF-1 receptor signaling in myeloid cells. *Cold Spring Harb. Perspect. Biol.* 6:a021857. https://doi.org/10.1101/cshperspect.a021857

Subramanian, A., P. Tamayo, V.K. Mootha, S. Mukherjee, B.L. Ebert, M.A. Gillette, A. Paulovich, S.L. Pomeroy, T.R. Golub, E.S. Lander, and J.P. Mesirov. 2005. Gene set enrichment analysis: a knowledge-based approach for interpreting genome-wide expression profiles. *Proc. Natl. Acad. Sci. USA*. 102:15545–15550. https://doi.org/10.1073/pnas.0506580102

Suttles, J., and R.D. Stout. 2009. Macrophage CD40 signaling: a pivotal regulator of disease protection and pathogenesis. *Semin. Immunol.* 21:257–264. https://doi.org/10.1016/j.smim.2009.05.011

Tamura, T., and K. Ozato. 2002. ICSBP/IRF-8: its regulatory roles in the development of myeloid cells. *J. Interferon Cytokine Res.* 22:145–152. https://doi.org/10.1089/107999002753452755

Topalian, S.L., C.G. Drake, and D.M. Pardoll. 2015. Immune checkpoint blockade: a common denominator approach to cancer therapy. *Cancer Cell*. 27:450–461. https://doi.org/10.1016/j.ccell.2015.03.001

Tumeh, P.C., C.L. Harview, J.H. Yearley, I.P. Shintaku, E.J. Taylor, L. Robert, B. Chmielowski, M. Spasic, G. Henry, V. Ciobanu, et al. 2014. PD-1 blockade induces responses by inhibiting adaptive immune resistance. *Nature*. 515:568–571. https://doi.org/10.1038/nature13954

Tutt, A.L., L. O'Brien, A. Hussain, G.R. Crowther, R.R. French, and M.J. Glennie. 2002. T cell immunity to lymphoma following treatment with anti-CD40 monoclonal antibody. *J. Immunol.* 168:2720–2728. https://doi.org/10.4049/jimmunol.168.6.2720

van der Sluis, T.C., M. Sluijter, S. van Duikeren, B.L. West, C.J. Melief, R. Arens, S.H. van der Burg, and T. van Hall. 2015. Therapeutic Peptide Vaccine-Induced CD8 T Cells Strongly Modulate Intratumoral Macrophages Required for Tumor Regression. *Cancer Immunol. Res.* 3:1042–1051. https://doi.org/10.1158/2326-6066.CIR-15-0052

Vonderheide, R.H., and M.J. Glennie. 2013. Agonistic CD40 antibodies and cancer therapy. *Clin. Cancer Res.* 19:1035–1043. https://doi.org/10.1158/1078-0432.CCR-12-2064

Wang, Q., and J. Liu. 2016. Regulation and Immune Function of IL-27. *Adv. Exp. Med. Biol.* 941:191–211. https://doi.org/10.1007/978-94-024-0921-5_9

Wiehagen, K.R., N.M. Girgis, D.H. Yamada, A.A. Smith, S.R. Chan, I.S. Grewal, M. Quigley, and R.I. Verona. 2017. Combination of CD40 agonism and CSF-1R blockade reconditions tumor-associated macrophages and drives potent antitumor immunity. *Cancer Immunol. Res.* 5:1109–1121; epub ahead of print. https://doi.org/10.1158/2326-6066.CIR-17-0258

Zhang, Q.W., L. Liu, C.Y. Gong, H.S. Shi, Y.H. Zeng, X.Z. Wang, Y.W. Zhao, and Y.Q. Wei. 2012. Prognostic significance of tumor-associated macrophages in solid tumor: a meta-analysis of the literature. *PLoS One*. 7:e50946. https://doi.org/10.1371/journal.pone.0050946

Zhu, Y., B.L. Knolhoff, M.A. Meyer, T.M. Nywening, B.L. West, J. Luo, A. Wang-Gillam, S.P. Goedegebuure, D.C. Linehan, and D.G. DeNardo. 2014. CSF1/CSF1R blockade reprograms tumor-infiltrating macrophages and improves response to T-cell checkpoint immunotherapy in pancreatic cancer models. *Cancer Res.* 74:5057–5069. https://doi.org/10.1158/0008-5472.CAN-13-3723

876

Short-term TAM hyperactivation by anti–CSF-1R+CD40 | Hoves et al.